A Mach-Sensitive Splitting Approach for Euler-like Systems

David Iampietro, Frédéric Daude, Pascal Galon, Jean-Marc Hérard

A Mach-Sensitive Splitting Approach for Euler-like Systems

D. Iampietro [*1,3,4], F. Daude [†1,3], P. Galon [‡3,5], and J-M Hérard [§2,4]

[1] *EDF lab Saclay, 7 boulevard Gaspard Monge 92120 Palaiseau, France*
[2] *EDF lab Chatou, 6 Quai Watier 78400 Chatou, France*
[3] *IMSIA, UMR EDF/CNRS/CEA/ENSTA 9219 Université Paris Saclay 828 Boulevard des Maréchaux 91762 Palaiseau Cedex, France*
[4] *I2M, UMR CNRS 7373 Technopôle Château-Gombert 39, rue F. Joliot Curie 13453 Marseille Cedex 13, France*
[5] *CEA DEN/DANS/DM2S/SEMT/DYN, D36 91190 Saclay, France*

February 13, 2017

Herein, a Mach-sensitive fractional step approach is proposed for Euler-like systems. The key idea is to introduce a time-dependent splitting which dynamically decouples convection from acoustic phenomenon following the fluctuations of the flow Mach number. By doing so, one seeks to maintain the accuracy of the computed solution for all Mach number regimes. Indeed, when the Mach number takes high values, a time-explicit resolution of the overall Euler-like system is entirely performed in one of the present splitting step. On the contrary, in the low-Mach number case, convection is totally separated from the acoustic waves production. Then, by performing an appropriate low-Mach correction on the acoustic step of the splitting, the numerical diffusion can be significantly reduced. A study made on both convective and acoustic subsystems of the present approach has revealed some key properties as hyperbolicity and positivity of the density and internal energy in the case of an ideal gas thermodynamics. The one-dimensional results made on a wide range of Mach numbers using an ideal and a stiffened gas thermodynamics show that the present approach is as accurate and CPU-consuming as a state of the art Lagrange-Projection-type method.

1 Introduction

In the following paper, Euler-like systems similar to homogeneous models [10] used for the two-phase flow simulation are at stake. The considered flows have their reference Mach number M varying between zero and arbitrary high values as time goes on.

[*] david.iampietro@edf.fr; Corresponding author
[†] frederic.daude@edf.fr
[‡] pascal.galon@cea.fr
[§] jean-marc.herard@edf.fr

If Godunov-like schemes manage to capture the compressible solutions in highly subsonic, sonic or supersonic regimes, stationary cases presented in [25, 24] show that they fail to be accurate in the case of low-Mach number flows on coarse meshes. Different related aspects can be tackled in order to elaborate a cure.

The first issue raising when M tends towards zero is related to the constraints on the discrete timestep Δt brought by Godunov-like schemes. Indeed, consider a wave whose propagation speed is σ; and consider the Courant number $C^\sigma = |\sigma| \, \Delta t/\Delta x$ associated to it; Δx being the spacestep of the computational domain. Then, if a time-explicit scheme such that $C^\sigma \ll 1$ is performed, σ-like waves will be depreciated by the spatial diffusive operator, whatever its amplitude, because of a too important number of timesteps to reach the end of the computation. Besides, as presented in [32, 15], studies made on linear wave equations suggest that implicit-time resolutions such that $C^\sigma \gg 1$ trigger a diffusion and a dispersion error on σ-like waves. Similar results found in the non-linear Euler system framework are presented in [40]. Therefore, if time-explicit Godunov-like schemes are applied to solve Euler-like systems in the case of low-Mach number flows, a natural stability condition is: $C^{|u|+c} = 1/2$; with u the speed of material-waves and c the flow speed of sound characterizing shock-wave front velocities. What is more, $C^{|u|}/C^{|u|+c} = M/(1+M)$ leading to $C^{|u|} \ll 1$. Thus, the material waves are largely damped. Besides, if the acoustic part of the system associated with c is solved using an implicit time integration, then $C^{|u|} \approx 1$, leading to $C^{|u|+c} \gg 1$. Hence, material-wave accuracy is improved but shock waves might be depreciated.

Unfortunately, when the fluid considered is slightly compressible as water, strong shock waves can occur even in low-Mach flow regimes [36]. In that case, one wishes to be accurate on the slow material waves as well as the fast and strong shock waves.

A second issue met in low-Mach number regimes is that Godunov-like schemes are not able to maintain an initial incompressible solution in the incompressible phase-space from one timestep to another. One way to overcome this difficulty is to apply preconditioning methods on the viscosity matrix of such schemes as in [43, 25, 24, 10]. More recently, the Asymptotic-Preserving (AP) approaches are designed such that their non-dimensional discretization is consistent with the asymptotic incompressible equations at low Mach number. In [16, 26, 19], the authors derive an implicit-explicit AP scheme based on a parametrized splitting of the conservative system. It results in a time-explicit resolution of a "slow" convective part of the system and a time-implicit treatment of a "fast" acoustic one.

A third low-Mach number difficulty related to the incompressible phase-space invariance is the spatial numerical diffusion. Indeed, in [17, 18], by transposing the theory of Schochet [33, 34] at the discrete level on the linearized barotropic Euler system, the authors prove that the non-centered terms in the acoustic flux of Godunov-like solvers produce a spatial non-dimensional numerical diffusion of order $O(\Delta x/M)$. Thus, as M tends towards zero, the discrete solution on coarse meshes suffers from an important lack of accuracy. The proposed remedy consists in adding a correction proportional to the local Mach number in front of the acoustic non-centered terms in the momentum equation.

This paper focuses essentially on the last issue described above but provides ideas to

tackle the first one too. Indeed, a Weighted Splitting Approach (WSA) is proposed in order to preserve accuracy for every Mach number regime. It has been inspired from [1] and [6] in which the Euler flux is split into a pure acoustic flux holding momentum and energy pressure terms, and a complementary convective flux. In order to circumvent the lack of hyperbolicity of the convective subsystem, the present approach introduces a time-weighted amount of pressure into the convective flux. Such a weighting parameter is sensitive to the time fluctuations of the maximal Mach number of the flow. Contrary to other splittings [45, 31, 41] which result in Flux-Vector Splitting (FVS) methods, the present work provides a fractional step approach which adapts itself dynamically to a wide range of flow behaviors. In the case of a low-Mach number flow, a correction of type [17, 18] or a straight implicitation of the acoustic flux similar to [13, 8] can be activated. Moreover, when M is close or superior to one, the splitting is cancelled and the overall Euler-like system is retrieved. The latter is solved using a Suliciu-like relaxation scheme [39] *without* any acoustic implicitation. Then, shock waves and sharp profiles are correctly captured. The fractional step approach as well as the space discretization of the present work are close to those introduced in [13, 8] in the context of a Lagrange-Projection method. Besides both methods provide numerical schemes whose writing is completely independent of the equation of state.

The paper is structured as follows: in section one, the dynamic splitting is firstly described at the continuous level. A study of each resulting conservative subsystem is done through hyperbolicity and positivity analyses. In section two, a special attention is paid to the non-dimensional version of both subsystems as well as their formal asymptotic behavior when the Mach number tends towards zero. Section three deals with the approximate Riemann solvers derived for the subsystems resolution. They stem from the relaxation scheme theory presented in [30, 9, 39, 4, 12]. Discrete positivity properties brought by the chosen discretization are also derived. Following the steps of [8], section four is devoted to different truncation error analyses. The dependence in terms of Mach number as well as the impact of the low-Mach correction on the numerical diffusive operator is shown. Eventually, section five presents one-dimensional explicit results obtained on a wide panel of Mach numbers and compared to the Lagrange-Projection method presented in [8].

2 Convective and Acoustic Effects in Euler-like Systems

2.1 Homogeneous Equilibrium Model Equations

When the non-equilibrium effects are small, one way to model two-phase flows is to assume that the two phases have the same velocity, pressure and temperature. The conservation laws are then similar to the Euler system. Define $\mathbf{U} = [\rho,\, \rho\,\mathbf{u},\, \rho\,e]^T$ the conservative

variables vector. In one space dimension, mass, momentum and energy conservation read:

$$\partial_t \rho + \underline{\nabla} \cdot (\rho \mathbf{u}) = 0, \tag{1a}$$
$$\partial_t (\rho \mathbf{u}) + \underline{\nabla} \cdot (\rho \mathbf{u} \otimes \mathbf{u} + p \mathbf{I}) = \mathbf{0}, \tag{1b}$$
$$\partial_t (\rho e) + \underline{\nabla} \cdot ((\rho e + p) \mathbf{u}) = 0, \tag{1c}$$
$$e = \frac{|\mathbf{u}|^2}{2} + \varepsilon, \ \varepsilon = \varepsilon^{EOS}(\rho, p), \tag{1d}$$
$$\rho c^2 = \left(\partial_p \varepsilon_{|\rho}\right)^{-1} \left(\frac{p}{\rho} - \rho \partial_\rho \varepsilon_{|p}\right). \tag{1e}$$

Equality in (1d) is the equation of state for a single phase fluid. It relates ε the specific internal energy with density and pressure. Its strong level of nonlinearity is known to produce rarefaction or shock waves inside the flow. Equation (1e) introduces c the sound speed which strongly depends on the fluid equation of state and governs the acoustic waves speed. Indeed let us recall that Euler system is strictly hyperbolic, its eigenvalues being in one-dimension: $\lambda_1^E = u - c < \lambda_2^E = u < \lambda_3^E = u + c$. What is more λ_1^E and λ_3^E are related to genuinely non-linear fields whereas λ_2^E is associated with a linearly degenerate one.

Eventually, let us write the second law of thermodynamics principle, introducing the specific entropy variable $s = s^{EOS}(\rho, \varepsilon)$ related with ρ and ε by the differential equation:

$$\begin{aligned} &d\varepsilon = T\, d s - p\, d\left(\frac{1}{\rho}\right), \\ &\text{with: } T = T^{EOS}(\rho, s) = \partial_s \varepsilon_{|\rho}, \ p = p^{EOS}(\rho, s) = \rho^2 \partial_\rho \varepsilon_{|s}. \end{aligned} \tag{2}$$

Using equation (2), it can be easily verified that, for smooth solutions, s is also solution of the PDE:

$$\partial_\rho s_{|p} + c^2 \partial_p s_{|\rho} = 0. \tag{3}$$

Such a physical entropy is used to characterise admissible weak solutions of Euler system (1). Indeed, as proved in [23], the mapping $(\rho, \rho \mathbf{u}, \rho e) \to -\rho s$ is a strictly convex function and $(-\rho s, -\rho \mathbf{u} s)$ constitutes a mathematical entropy pair. Thus, any admissible weak solution of the Euler system should verify the inequality:

$$\partial_t (\rho s) + \underline{\nabla} \cdot (\rho s \mathbf{u}) \geq 0. \tag{4}$$

Beyond conservativity and maximum principle, inequality (4) is a key theoretical property that one would like to obtain, at the discrete level, in a numerical scheme.

Let us end this subsection by defining the one-dimensional Riemann problem associated to system (1). Let $\mathbf{U}_L$ and $\mathbf{U}_R$ be two constant states of the one-dimensional Euler system (1). It reads:

$$\begin{aligned} &\partial_t \mathbf{U} + \partial_x \mathbf{F}(\mathbf{U}) = \mathbf{0}, \\ &\mathbf{U}(., t = 0) = \begin{cases} \mathbf{U}_L, \text{ if } x < 0 \\ \mathbf{U}_R, \text{ if } x > 0, \end{cases} \quad \text{with: } \mathbf{F}(\mathbf{U}) = \begin{bmatrix} \rho u \\ \rho u^2 + p \\ (\rho e + p) u \end{bmatrix}. \end{aligned} \tag{5}$$

As proved in [37], in the case of ideal gas or in [23] under more general thermodynamical hypothesis, Riemann problem (5) admits a unique entropic solution made of contact waves, rarefaction waves and shock waves as long as $\mathbf{U}_L$ and $\mathbf{U}_R$ are close enough.

2.2 A Weighted Splitting Approach

As mentioned in the introduction, different connected issues raise in the case of low-Mach number flows. First, as pointed out in [17], two different physics are at stake inside Euler-like systems. The first convects conservative variables using velocity u, the second contains pressure effects responsible for shock and rarefaction waves propagating at speed $u \pm c$. Thus, in the case of low-Mach flows, $|u| \ll c$ and the acoustic physics goes much faster than the convective one. Therefore, time-explicit schemes restricted by the acoustic CFL condition tend to diffuse material waves as time goes on. Secondly, as mentioned in [24], the projection step of the Riemann-like solvers introduces spurious acoustic waves which force the initial incompressible datum to leave the incompressible phase space after one timestep. Lastly, when a truncation error analysis is performed on smooth solutions got from Riemann-like solvers, one can notice [22, 8] that the non-centered terms in the momentum flux produce non-dimensional numerical diffusion of order $O(\Delta x/M)$, with M the flow Mach number. Hence, on coarse meshes, in the case of low-Mach flows, smooth solutions suffer from strong spatial numerical diffusion.

One can notice that the above three difficulties stem from the acoustic part of the conservative system. Thus, a first step to overcome these issues is to decouple the convective from the acoustic physics and proceed to their resolution separately. This can be done by splitting the Euler system into two new continuous subsystems:

$$\mathcal{C}: \begin{cases} \partial_t \rho + \underline{\nabla} \cdot (\rho \mathbf{u}) = 0, \\ \partial_t (\rho \mathbf{u}) + \underline{\nabla} \cdot \Big(\rho \mathbf{u} \otimes \mathbf{u} + \mathscr{E}_0^2(t)\, p \mathbf{I}\Big) = \mathbf{0}, \\ \partial_t (\rho e) + \underline{\nabla} \cdot \Big((\rho e) + \mathscr{E}_0^2(t)\, p\Big) \mathbf{u}\Big) = 0, \end{cases} \quad \mathcal{A}: \begin{cases} \partial_t \rho = 0, \\ \partial_t (\rho \mathbf{u}) + \underline{\nabla} \cdot \Big((1 - \mathscr{E}_0^2(t))\, p \mathbf{I}\Big) = \mathbf{0}, \\ \partial_t (\rho e) + \underline{\nabla} \cdot \Big((1 - \mathscr{E}_0^2(t))\, p \mathbf{u}\Big) = 0. \end{cases} \tag{6}$$

(7)

Here, $\mathscr{E}_0(.)$ is a time-dependent weighting factor belonging to interval $]0, 1]$. Details about how to build such a parameter will be given later; but one should keep in mind that:

$$\begin{aligned} &\mathscr{E}_0(t) \propto \min\left(M_{max}^{\alpha}(t),\, 1\right), \\ &M_{max}(t) = \sup_{x \in \Omega} \left(M(x,t) = \frac{|u(x,t)|}{c(x,t)}\right), \end{aligned} \tag{8}$$

Ω being the computational domain and $\alpha > 0$ an appropriate power which will be chosen in **Section 5**.

First of all, one can notice that formally summing conservative subsystems $\mathcal{C}$ and $\mathcal{A}$ allows to recover the original Euler system (1). Suppose that at instant t the flow is such that $M_{max}(t)$ is close or superior to 1. Then, $\mathscr{E}_0(t)$ will be close to 1, the subsystem $\mathcal{C}$ formally converges towards the full Euler system while $\mathcal{A}$ is a degenerated stationary subsystem. Hence, if $\mathcal{C}$ is solved using a time-explicit Godunov-like scheme, Euler shocks

would be correctly captured. On the contrary, In the case of a globally low-Mach number flow, $M_{max}(t) \approx \mathscr{E}_0(t) \ll 1$, and pressure terms completely disappear from $\mathcal{C}$ which turns out to be a pure "convective" subsystem. Pressure terms are treated afterwards in $\mathcal{A}$ which becomes an "acoustic" subsystem. Particularly, in the case of low-Mach number flows, a correction of type [22, 8, 18] would tackle the spatial numerical diffusion while a straight implicitation [13, 19] would remove the most constraining part of the CFL condition.

In the sequel, $\mathcal{C}$ is referred as the convective subsystem and $\mathcal{A}$ the acoustic one. Before going further into the numerical resolution of $\mathcal{C}$ and $\mathcal{A}$, one has to study their basic mathematical properties: hyperbolicity and maximum principle. This is done in the next section.

2.2.1 Hyperbolicity of $\mathcal{C}$ and $\mathcal{A}$

Above all, the hyperbolicity of the two subsystems $\mathcal{C}$ and $\mathcal{A}$ is investigated. This ensures that solutions of $\mathcal{C}$ and $\mathcal{A}$ do not suffer from definition issues by producing waves with celerities evolving in the $\mathbb{C}$ space. This is the object of the following proposition written in one space dimension but easily extendable to the multi-dimensional case:

Proposition 1 (Hyperbolicity of convective and acoustic subsystems)**.** *Let us introduce $c_{\mathcal{C}}(\rho, p)$ and $c_{\mathcal{A}}(\rho, p)$ two modified sound speeds such that:*

$$\begin{aligned} (\rho\, c_{\mathcal{C}}(\rho, p))^2 &= \left(\partial_p \varepsilon_{|\rho}\right)^{-1} \left(\mathscr{E}_0^2\, p - \rho^2\, \partial_\rho \varepsilon_{|p}\right), \\ (\rho\, c_{\mathcal{A}}(\rho, p))^2 &= \left(\partial_p \varepsilon_{|\rho}\right)^{-1} p. \end{aligned} \tag{9}$$

In the case of a stiffened gas thermodynamics, $c_{\mathcal{C}}^2 \geq 0$. Besides, if pressure remains positive, $c_{\mathcal{A}}^2 \geq 0$. Under this condition, the subsystems $\mathcal{C}$ and $\mathcal{A}$ are hyperbolic. Their eigenvalues are:

$$\begin{aligned} \lambda_1^{\mathcal{C}} &= u - \mathscr{E}_0\, c_{\mathcal{C}} && \leq \lambda_2^{\mathcal{C}} = u \leq \lambda_3^{\mathcal{C}} = u + \mathscr{E}_0\, c_{\mathcal{C}}, \\ \lambda_1^{\mathcal{A}} &= -\left(1 - \mathscr{E}_0^2\right) c_{\mathcal{A}} && \leq \lambda_2^{\mathcal{A}} = 0 \leq \lambda_3^{\mathcal{A}} = \left(1 - \mathscr{E}_0^2\right) c_{\mathcal{A}}, \end{aligned} \tag{10}$$

the 1-wave and 3-wave of both subsystems are associated to genuinely non-linear fields whereas the 2-wave field are linearly degenerate. What is more, $c_{\mathcal{C}}$, $c_{\mathcal{A}}$ and c are related by:

$$(c_{\mathcal{C}})^2 + \left(1 - \mathscr{E}_0^2\right) (c_{\mathcal{A}})^2 = c^2. \tag{11}$$

The proof of this proposition is written in Appendix A. Beside, using relation (11), it can be observed that, when $\mathscr{E}_0$ is close to one, $\mathcal{C}$ is approximately equivalent to the Euler system, and that is why: $\forall k$, $\lim\limits_{\mathscr{E}_0 \to 1} \lambda_k^{\mathcal{C}} = \lambda_k^E$. Moreover, when $\mathscr{E}_0$ tends towards zero, $\lim\limits_{\mathscr{E}_0 \to 0} \lambda_k^{\mathcal{C}} = \lambda_2^E = u$, because of the pressure terms disappearance. $\mathcal{C}$ then degenerates into a pure convective subsystem already exhibited in [1, 6]. However, $\forall k \in \{1, 3\}$: $\left|\lambda_k^{\mathcal{C}}\right| \leq \left|\lambda_k^E\right|$ and $\left|\lambda_k^{\mathcal{A}}\right| \leq c$ even when $\mathscr{E}_0$ goes to zero. Thus, the weighted splitting approach always tends

to underestimate convective and acoustic wave speeds whatever is the thermodynamics. This can be clearly seen in the case of ideal gas:

$$\begin{aligned} c_{\mathcal{C}} &= \sqrt{\frac{\gamma_{\mathscr{E}_0}\, p}{\rho}},\ \gamma_{\mathscr{E}_0} = \mathscr{E}_0^2\ (\gamma-1)+1 \leq \gamma, \\ c_{\mathcal{A}} &= \sqrt{\frac{(\gamma-1)\ p}{\rho}} < c = \sqrt{\frac{\gamma\, p}{\rho}}. \end{aligned} \tag{12}$$

In **Section 4**, the transcription, at discrete level, of these non physical wave speeds will be seen. A numerical way to bypass this difficulty and follow the real physics will also be proposed.

2.2.2 Positivity of Density and Internal Energy

Positivity requirements reflect the invariance of a given solution towards its thermodynamical phase space. In this study, one focuses on the ideal (IG) and the stiffened gas (SG) thermodynamics defined by the following phase-spaces:

$$\rho\,\varepsilon = \frac{p}{(\gamma-1)}, \tag{13a}$$

$$\Phi_{PG} = \left\{ \mathbf{U},\ e = \frac{|\mathbf{u}|^2}{2} + \varepsilon,\ \rho > 0,\ \rho\,\varepsilon > 0 \right\}, \tag{13b}$$

$$= \left\{ \mathbf{U},\ e = \frac{|\mathbf{u}|^2}{2} + \varepsilon,\ \rho > 0,\ p > 0 \right\}, \tag{13c}$$

$$\rho\,\varepsilon = \frac{p+\gamma\, P_\infty}{(\gamma-1)}, \tag{14a}$$

$$\Phi_{SG} = \left\{ \mathbf{U},\ e = \frac{|\mathbf{u}|^2}{2} + \varepsilon,\ \rho > 0,\ \rho\,\varepsilon > P_\infty \right\}, \tag{14b}$$

$$= \left\{ \mathbf{U},\ e = \frac{|\mathbf{u}|^2}{2} + \varepsilon,\ \rho > 0,\ p > -P_\infty \right\}. \tag{14c}$$

Consider Ω a spatial domain of boundary $\partial\Omega$. Define $\mathbf{n}$ the outward local normal vector of $\partial\Omega$. Let ϕ be a theoretically positive variable endowed with a positive inlet boundary condition: $\phi_{|\partial\,\Omega} \geq 0$ if $\mathbf{u}\cdot\mathbf{n}_{|\partial\,\Omega} \leq 0$; and an admissible initial condition: $\phi(.,t=0) \geq 0$. Then, as proved in [21] for sufficiently smooth solutions, positivity of density ρ is naturally obtained from mass equation in subsystem $\mathcal{C}$. Density is also stationary in subsystem $\mathcal{A}$. So, after having successively solved $\mathcal{C}$ and $\mathcal{A}$ density remains positive. Furthermore, internal energy in subsystem $\mathcal{C}$ and $\mathcal{A}$ verifies:

$$\begin{cases} \partial_t\,\varepsilon + \mathbf{u}\cdot\underline{\nabla}\varepsilon + \mathscr{E}_0^2(t)\,\dfrac{p}{\rho}\,\underline{\nabla}\cdot\,\mathbf{u} = 0, & (\mathcal{C}) \\ \partial_t\,\varepsilon + \left(1-\mathscr{E}_0^2(t)\right)\,\dfrac{p}{\rho}\,\underline{\nabla}\cdot\,\mathbf{u} = 0. & (\mathcal{A}) \end{cases} \tag{15}$$

By making the same kind of regularity hypothesis than in [21], one can prove that In the case of an ideal gas thermodynamics, ε remains positive on Ω throughout time. See Appendix B for more details. However, In the case of a stiffened gas thermodynamics (14a), this is $\dfrac{p+P_\infty}{\gamma-1} = \rho\,\varepsilon - P_\infty = P$ which has to remain positive. Unfortunately, the

PDE verified by this variable in $\mathcal{C}$ and $\mathcal{A}$ contains the term $P_\infty\left(1-\mathscr{E}_0^2\right)\underline{\nabla}\cdot\mathbf{u}$. Since $P_\infty\left(1-\mathscr{E}_0^2\right)/P$ is a priori unbounded, it is not possible to guarantee that the subsystems $\mathcal{C}$ and $\mathcal{A}$ preserve the phase space constraint $p\geq -P_\infty \Leftrightarrow P>0$ on Ω throughout time unless $\mathscr{E}_0=1$ which corresponds to the resolution of Euler system or $P_\infty=0$ which is the ideal gas case. More details are given in Appendix B.

Beyond the theoretical properties held by both $\mathcal{C}$ and $\mathcal{A}$, one is also interested in their asymptotic behavior in the case of low-Mach number flows. Details about this singular matter are given in the next section.

3 Low-Mach Number Asymptotic Behaviors

3.1 Non-dimensional Euler System

The low-Mach number issue deals with the asymptotic non-dimensional model of Euler system reached when the Mach number tends to zero. Let us recall that, provided an appropriate rescaling of the Euler system (1) (see [8]), one obtains a non-dimensional version which reads:

$$\partial_{\overline{t}}\,\overline{\rho}+\underline{\nabla}\cdot\left(\overline{\rho}\,\overline{\mathbf{u}}\right)=0, \tag{16a}$$

$$\partial_{\overline{t}}\left(\overline{\rho}\,\overline{\mathbf{u}}\right)+\underline{\nabla}\cdot\left(\overline{\rho}\,\overline{\mathbf{u}}\otimes\overline{\mathbf{u}}+\frac{\overline{p}}{M_r^2}\,\mathbf{I}\right)=\mathbf{0}, \tag{16b}$$

$$\partial_{\overline{t}}\left(\overline{\rho}\,\overline{e}\right)+\underline{\nabla}\cdot\left((\overline{\rho}\,\overline{e}+\overline{p})\underline{\overline{u}}\right)=0, \tag{16c}$$

$$\overline{e}=M_r^2\,\frac{\left|\overline{\mathbf{u}}\right|^2}{2}+\overline{\varepsilon},\ \overline{p}=\overline{p}^{EOS}\left(\overline{\rho},\,\overline{\varepsilon}\right). \tag{16d}$$

Here, $M_r=u_r/c_r$ is a reference Mach number made of a reference velocity out of a reference speed of sound. In the sequel, for the sake of simplicity, we drop the bars and rewrite M_r as M. In [35] and [34] the authors have proved that, in the case of well-prepared initial conditions:

$$\begin{aligned}&p(.,\,0)=p_0+O\left(M^2\right),\\&\mathbf{u}(.,\,0)=\mathbf{u}_0+O\left(M\right),\\&\text{with } p_0 \text{ constant and } \underline{\nabla}\cdot\left(\mathbf{u}_0\right)=0,\end{aligned} \tag{17}$$

the solution of system (16) converges towards the solution of the incompressible system when M tends to zero:

$$\partial_t\,\rho+\mathbf{u}\cdot\underline{\nabla}\,\rho=0 \tag{18a}$$

$$\rho\,\left(\partial_t\,\mathbf{u}+\mathbf{u}\cdot\underline{\nabla}\,\mathbf{u}\right)+\underline{\nabla}\,\pi=\mathbf{0} \tag{18b}$$

$$\underline{\nabla}\cdot\left(\mathbf{u}\right)=0 \tag{18c}$$

Here, $\pi=\underset{M\to 0}{lim}\,\dfrac{p-p_0}{M^2}$ is called hydrodynamic pressure. It is a completely independent unknown and plays the role of Lagrange multiplyer related to the incompressibility constraint

$\underline{\nabla} \cdot (\mathbf{u}) = 0$. It is worth considering both non-dimensional writings of subsystems $\mathcal{C}$ and $\mathcal{A}$. Particularly, by formally performing a Taylor expansion in Mach powers, one can assess how the Euler incompressible system has been split between both non-dimensional subsystems when the Mach number tends to zero.

3.2 Non-dimensional Convective Subsystem

The non-dimensional subsystem $\mathcal{C}$ reads:

$$\mathcal{C} : \begin{cases} \partial_t \rho + \underline{\nabla} \cdot (\rho \mathbf{u}) = 0, \\ \partial_t (\rho \mathbf{u}) + \underline{\nabla} \cdot (\rho \mathbf{u} \otimes \mathbf{u}) + \left(\dfrac{\mathscr{E}_0(t)}{M} \right)^2 \underline{\nabla} p = \mathbf{0}, \\ \partial_t (\rho e) + \underline{\nabla} \cdot \Big((\rho e) + \mathscr{E}_0^2(t)\, p) \mathbf{u} \Big) = 0, \\ e = M^2 \dfrac{|\mathbf{u}|^2}{2} + \varepsilon, \ p = p^{EOS}(\rho, \varepsilon). \end{cases} \tag{19}$$

As it can be seen, the weighting factor $\mathscr{E}_0$ comes to compensate the $1/M$ dependency in front of pressure term in the momentum equation of $\mathcal{C}$. Let us suppose that $\mathscr{E}_0(t)$ is of order M and introduce $\overline{\mathscr{E}}_0$ such that, $\mathscr{E}_0 = M\, \overline{\mathscr{E}}_0$, $\overline{\mathscr{E}}_0 = O(1)$. As previously announced, let us perform a Mach expansion for any variable ϕ belonging to $\{\rho, u, p, e, \varepsilon\}$:

$$\phi = \phi_0 + M\, \phi_1 + M^2\, \phi_2 + O(M^3)$$

Then, one can formally observe that, at zero order:

$$\mathcal{C}^0 : \begin{cases} \partial_t \rho_0 + \underline{\nabla} \cdot (\rho_0 \mathbf{u}_0) = 0 \\ \partial_t (\rho_0 \mathbf{u}_0) + \underline{\nabla} \cdot (\rho_0 \mathbf{u}_0 \otimes \mathbf{u}_0) + \overline{\mathscr{E}}_0(t)^2\, \underline{\nabla} p_0 = \mathbf{0} \\ \partial_t (\rho_0 \varepsilon_0) + \underline{\nabla} \cdot (\rho_0 \varepsilon_0 \mathbf{u}_0) = 0 \end{cases} \tag{20}$$

Combining mass equation with internal energy equation in $\mathcal{C}^0$ one can notice that: $\dfrac{\mathrm{d}\varepsilon_0}{\mathrm{d}t} = 0$. At zero order, the internal energy solution of the convective subsystem remains constant along the fluid streamlines. Thus, if initially internal energy is constant over all the domain, it will remain constant throughout the time. In that case, one can write:

$$\varepsilon^{EOS}(\rho_0, p_0) = \varepsilon_0 \ (constant) \Leftrightarrow p_0 = p^{EOS}(\rho_0) \tag{21}$$

under the hypothesis that $\partial_\rho \varepsilon^{EOS}_{|p}(\rho_0, p_0) \neq 0$. Then , $\mathcal{C}^0$ can be viewed as a non-dimensional barotropic system:

$$\left(\mathcal{C}^0\right)_{M \to 0} \begin{cases} \partial_t \rho_0 + \underline{\nabla} \cdot (\rho_0 \mathbf{u}_0) = 0 \\ \partial_t (\rho_0 \mathbf{u}_0) + \underline{\nabla} \cdot (\rho_0 \mathbf{u}_0 \otimes \mathbf{u}_0) + \overline{\mathscr{E}}_0(t)^2\, \underline{\nabla} p(\rho_0) = \mathbf{0} \end{cases} \tag{22}$$

3.3 Non-dimensional Acoustic Subsystem

The non-dimensional acoustic subsystem $\mathcal{A}$ can be written:

$$\mathcal{A}: \begin{cases} \partial_t \rho = 0, \\ \partial_t (\rho \mathbf{u}) + \dfrac{(1-\mathscr{E}_0^2(t))}{M^2} \underline{\nabla} p = \mathbf{0}, \\ \partial_t (\rho e) + \underline{\nabla} \cdot \left((1-\mathscr{E}_0^2(t)) p \mathbf{u} \right) = 0, \\ e = M^2 \dfrac{|\mathbf{u}|^2}{2} + \varepsilon, \ p = p^{EOS}(\rho, \varepsilon). \end{cases} \tag{23}$$

Using the same Mach expansion than previously, it can be noticed that, at zero order:

$$\mathcal{A}^0: \begin{cases} \partial_t \rho_0 = 0, \\ \underline{\nabla} (p_0 + M p_1) = \mathbf{0}, \\ \partial_t (\rho_0 \varepsilon_0) + \underline{\nabla} \cdot (p_0 \mathbf{u}_0) = 0. \end{cases} \tag{24}$$

Contrary to $\mathcal{C}^0$, momentum equation in $\mathcal{A}^0$ allows to write pressure as:

$$p = p_0(t) + M^2 p_2 + O(M^3) \tag{25}$$

Pressure equation at zero order for smooth solutions gives:

$$\frac{-\dfrac{\mathrm{d}p_0}{\mathrm{d}t}(t)}{\rho_0 c_{\mathcal{A}}(\rho_0, p_0)^2} = \underline{\nabla} \cdot \mathbf{u}_0 \tag{26}$$

By integrating over the whole spatial domain and imposing no-slip boundary conditions one obtains:

$$\begin{aligned} &\frac{\mathrm{d}p_0}{\mathrm{d}t}(t) = 0 \Leftrightarrow p = \overbrace{p_0}^{constant} + M^2 p_2 + O(M^3) \\ &\underline{\nabla} \cdot \mathbf{u}_0 = 0 \end{aligned} \tag{27}$$

Thus, at zero order, solutions of the acoustic subsystem tend "formally" to be solution of:

$$\left(\mathcal{A}^0\right)_{M\to 0}: \begin{cases} \rho_0 = \rho_0(\mathbf{x}), \\ \rho_0 \partial_t \mathbf{u}_0 + \underline{\nabla} p_2 = \mathbf{0}, \\ \underline{\nabla} \cdot \mathbf{u}_0 = 0. \end{cases} \tag{28}$$

The above asymptotic system has the particularity to be independent of the weighted splitting parameter $\overline{\mathscr{E}}_0$ and looks like an incompressible convection-free system.

Remark 1. *One should keep in mind that the above derivations of subsystems* $\left(\mathcal{C}^0\right)_{M\to 0}$ *and* $\left(\mathcal{A}^0\right)_{M\to 0}$ *are only formal. Theory allowing to prove the convergence of the compressible Euler system towards its incompressible equivalent is extremely complex and requires energy*

manipulations which are not considered here. We only see the above calculations as keys to interpret physically the behavior of the splitting operator process. Particularly, at low-Mach number, momentum evolutions in the convective subsystem seems to be essentially caused by momentum convection and by the small density fluctuations. On the contrary, in the acoustic subsystem, one could say that momentum dynamic is exactly balanced by strong incompressible pressure forces. Hence, one could expect that the low-Mach numerical issues happen during the acoustic resolution.

In the following, the derivation of the numerical scheme is described.

4 Relaxation Scheme Applied to the Weighted Splitting Approach

For the sake of simplicity and with no loss of generality, the scheme description is done in one dimension. Literature dealing with relaxation schemes is vast. Without being exhaustive, we refer to [30] for the derivation of relaxation schemes applied to abstract hyperbolic systems in which the whole flux is relaxed. In [9], the authors question the existence of solutions for the relaxation systems as well as their convergence towards a local equilibrium. A detailed study of the entropy-satisfying relaxation method applied to the isentropic gas dynamics system and extended to the fully compressible Euler system is given in [5]. It uses a Suliciu-like relaxation technique [39] which is also applied in [2] on a Drift-Flux model. Besides, the acoustic part of the Lagrange-Projection splitting derived in [22, 8] is solved the same way too. Eventually in [12], an extension of the Suliciu approach to general fluid systems is done. Following the same approach, we proceed to a Suliciu-like relaxation method on both subsystems $\mathcal{C}$ and $\mathcal{A}$.

Let us recall that the Suliciu relaxation method applied on Euler-like systems consists in introducing a new pressure variable Π endowed with a "quasi-linear" dynamics converging towards the real pressure variable p. This convergence is ensured thanks to a source term whose timescale $\mu \ll 1$. The new system is still hyperbolic and has only linearly degenerate fields which makes the derivation of an exact Godunov solver easier. What is more, the high level of nonlinearity brought by the pressure variable via the equation of state (1d) is encapsulated in one single constant. As a consequence, the derivation of the numerical scheme can be done independently of the thermodynamics law. The cost to be paid is the increase of the system dimension through an additional equation for Π. What is more, one has to decide how to treat the equilibrium between Π and p numerically.

4.1 Suliciu Relaxation for the Weighted Splitting Approach

Using internal energy equations (15) associated with the equation of state, one can derive the following pressure PDEs for both subsystems $\mathcal{C}$ and $\mathcal{A}$:

$$\mathcal{C}: \ \partial_t p + u\,\partial_x p + \rho\,(c_{\mathcal{C}})^2\,\partial_x u = 0, \tag{29}$$

$$\mathcal{A}: \ \partial_t p + (1-\mathscr{E}_0^2)\,\rho\,(c_{\mathcal{A}})^2\,\partial_x u = 0. \tag{30}$$

Then, replace pressure $p(\rho, \varepsilon)$ by a new relaxation pressure variable Π which no longer depends of density and internal energy. One also expects Π to mimic the above physical pressure dynamics but with an additional linearization effect on the thermodynamics. This is done by introducing two constants $a_{\mathcal{C}} > 0$ and $a_{\mathcal{A}} > 0$ such that Π verifies:

$$\mathcal{C}: \ \partial_t \Pi + u\,\partial_x \Pi + \frac{a_{\mathcal{C}}^2}{\rho}\partial_x u = \frac{(p-\Pi)}{\mu}, \quad \mathcal{A}: \ \partial_t \Pi + (1-\mathscr{E}_0^2)\,\frac{a_{\mathcal{A}}^2}{\rho}\partial_x u = \frac{(p-\Pi)}{\mu}. \tag{31}$$ (32)

Here, $a_{\mathcal{C}}$ (respectively $a_{\mathcal{A}}$) is homogeneous to a density times a velocity and encapsulates the non-linear effects brought by $\rho\, c_{\mathcal{C}}(\rho, \varepsilon)$ (respectively $\rho\, c_{\mathcal{A}}(\rho, \varepsilon)$). Besides, by using the mass equation, it is possible to rewrite equations (31) and (32) in a conservative way namely:

$$\mathcal{C}: \ \partial_t(\rho\Pi) + \partial_x\left((\rho\Pi + a_{\mathcal{C}}^2)\,u\right) = \frac{\rho\,(p-\Pi)}{\mu}, \ \mathcal{A}: \ \partial_t(\rho\Pi) + \partial_x\left((1-\mathscr{E}_0^2)a_{\mathcal{A}}^2\,u\right) = \frac{\rho\,(p-\Pi)}{\mu}. \tag{33}$$ (34)

One can observe that, when $\mu \to 0$ in (31) and (32), the relaxation pressure Π tends formally towards p at order zero in μ. Hence $(p-\Pi)/\mu$ can be formally interpreted as a correction term of time scale μ forcing the relaxation pressure to converge towards the physical pressure instantaneously if μ tends to zero.

Finally, the relaxation convective and acoustic systems read:

$$\mathcal{C}^\mu: \begin{cases} \partial_t \rho + \partial_x(\rho u) = 0, \\ \partial_t(\rho u) + \partial_x\left(\rho u^2 + \mathscr{E}_0^2(t)\,\Pi\right) = 0, \\ \partial_t(\rho e) + \partial_x\left((\rho e + \mathscr{E}_0^2(t)\,\Pi)\,u\right) = 0, \\ \partial_t(\rho\Pi) + \partial_x\left((\rho\Pi + a_{\mathcal{C}}^2)\,u\right) = \dfrac{\rho\,(p-\Pi)}{\mu}. \end{cases} \quad \mathcal{A}^\mu: \begin{cases} \partial_t \rho = 0, \\ \partial_t(\rho u) + \partial_x\left((1-\mathscr{E}_0^2(t))\,\Pi\right) = 0, \\ \partial_t(\rho e) + \partial_x\left((1-\mathscr{E}_0^2(t))\,\Pi\,u\right) = 0, \\ \partial_t(\rho\Pi) + \partial_x\left((1-\mathscr{E}_0^2(t))\,a_{\mathcal{A}}^2\,u\right) = \dfrac{\rho\,(p-\Pi)}{\mu}. \end{cases} \tag{35}$$ (36)

Remark 2. *It is worth noting that, in the derivation of the convective and acoustic relaxation subsystems it would have been possible to skip the forcing term $(p-\Pi)/\mu$. Indeed, following [4], one could have simply introduced the notion of projection on the Maxwellian equilibrium.*

One way to calibrate the constant relaxation coefficient $a_{\mathcal{C}}$ (respectively $a_{\mathcal{A}}$) is to perform a Chapman-Enskog expansion by rewriting all the variables $\phi \in \{\rho, u, e, \Pi\}$ in power of μ:

$$\begin{aligned} &\phi = \phi_0 + \mu\,\phi_1 + \mu^2\,\phi_2 + .., \\ &\Pi_0 = p. \end{aligned}$$

By doing so, one can exhibit a subcharacteristic-like condition, also called Whitham-like condition [44]. It allows to prevent $\mathcal{C}^\mu$ (respectively $\mathcal{A}^\mu$) from triggering instabilities when $\mu \to 0$. What is more, it can be used as a sufficient condition to build an entropy pair and an extended entropy inequality for the relaxation system (see [9, 5]). As detailed in

Appendix E, the subcharacteristic conditions obtained are:

$$\mathcal{C}^{\mu}: \; a_{\mathcal{C}} > \rho\, c_{\mathcal{C}} \tag{37a}$$

$$\mathcal{A}^{\mu}: \; a_{\mathcal{A}} > \rho\, c_{\mathcal{A}} \tag{37b}$$

Remark 3. *By proceeding in the same manner, one could have obtained a Suliciu-like relaxation Euler system. The relaxation pressure PDE would have been:*

$$\partial_t \Pi + u\, \partial_x \Pi + \frac{a_E^2}{\rho}, \partial_x u = \frac{(p - \Pi)}{\mu}, \tag{38}$$

with a_E the constant relaxation coefficient constrained by the Euler subcharacteristic condition:

$$a_E > \rho\, c. \tag{39}$$

Recall that $\lim_{\mathscr{E}_0 \to 1} c_{\mathcal{C}} = c$, and then (37a) *becomes* (39) *in that case. More generally, the shape of such a Suliciu-like relaxation Euler system can be obtained by formally making $\mathscr{E}_0$ tend towards one in $\mathcal{C}^{\mu}$.*

Remark 4. *In [11], [5], [7], [13] and [12], in order to solve the Euler system using relaxation techniques, the authors perform an inversion between the role played by total energy and entropy. The idea is to turn the total energy equation into a mathematical entropy constraint while injecting the pure transport entropy equation:*

$$\partial_t s + u\, \partial_x s = 0. \tag{40}$$

By doing so, one can lean on good properties brought by relaxation methods applied on the barotropic Euler system and enforce the entropy inequality (4) *in the numerical resolution of the full Euler system. More details can be found in the above references. In our splitting approach, such a strategy is avoided. Indeed, it can be shown that the physical entropy function $\mathbf{U} \to s(\mathbf{U})$ defined in equation* (3) *does no longer verify equation* (40) *when $\mathbf{U}$ is solution of both subsystems $\mathcal{C}$ and $\mathcal{A}$. An additional non-conservative term appears and prevents from applying directly the barotropic-relaxation system results. That is why, in our case, a simple Suliciu-relaxation method is performed on the conservative system including total energy. Note that a similar relaxation treatment is done in [8] for the acoustic subsystem.*

Remark 5. *As previously noted in* ***Subsection 2.2.1****, the lower bound in the acoustic subcharacteristic condition* (37b) *uses an artificial celerity naturally provided by subsystem $\mathcal{A}$. In the case of an ideal or a stiffened gas thermodynamics, $c_{\mathcal{A}} < c$, and inequality* (37b) *could violate the natural acoustic subcharacteristic condition* (39) *based on the real sound speed which is found in [7], [13] and [22].*

So far, no theoretical results allowing to prove the stability of the overall weighted splitting approach under condition (37b) *have been found. However, from a numerical point of view, we think that it is relevant and easy to compare conditions* (37b) *and* (39)*. This will be done in* ***Subsection 6.2****.*

4.2 Derivation of the Relaxation Scheme

Let us define Δx (respectively Δt) the space step (respectively the time step) of the scheme. For $i \in [1, .., N_{cells}]$ let us set $x_i = i\,\Delta x$, the coordinate of the cell center i and $x_{i+1/2} = x_i + \Delta x/2$, the coordinate of face $i + 1/2$. Let us consider $\mathbf{W} = [\rho,\, \rho\, u,\, \rho\, e,\, \rho\, \Pi]^T$ the extended relaxation conservative vector. The Riemann problem related to (35) or (36) writes:

$$\partial_t\, \mathbf{W} + \partial_x\, \mathbf{F}^\mu\,(\mathbf{W}) = \mathbf{S}^\mu\,(\mathbf{W}) \qquad \mathbf{W}(t=0,.) = \begin{cases} \mathbf{W}_L \text{ if } x < 0 \\ \mathbf{W}_R \text{ if } x > 0 \end{cases} \tag{41}$$

With $\mathbf{S}^\mu\,(\mathbf{W}) = \begin{bmatrix} 0 \\ 0 \\ 0 \\ \rho\,(p-\Pi)/\mu \end{bmatrix}$ and $\mathbf{F}^\mu \in \left\{ \mathbf{F}^\mu_{\mathcal{C}}\,(\mathbf{U}) = \begin{bmatrix} \rho\, u \\ \rho\, u^2 + \mathscr{E}_0^2\, \Pi \\ (\rho\, e + \mathscr{E}_0^2\, \Pi)\, u \\ (\rho\, \Pi + (a_{\mathcal{C}})^2)\, u \end{bmatrix},\ \mathbf{F}^\mu_{\mathcal{A}}\,(\mathbf{U}) = (1-\mathscr{E}_0^2) \begin{bmatrix} 0 \\ \Pi \\ \Pi\, u \\ (a_{\mathcal{A}})^2\, u \end{bmatrix} \right\}.$

Let us introduce $\mathbf{U}_i^{n+1}$ the discrete approximation of $\dfrac{1}{\Delta x} \displaystyle\int_{x_{i-1/2}}^{x_{i+1/2}} L(\mathbf{W}^{God}) \left(\frac{x}{t^{n+1}};\, \mathbf{W}_i^n,\, \mathbf{W}_{i+1}^n \right) dx$ on cell i at time $t^{n+1} = t^n + \Delta t$, $\mathbf{W}^{God}(.;\, \mathbf{W}_i^n,\, \mathbf{W}_{i+1}^n)$ being the self similar solution of the Riemann problem (41) and $L : \mathbf{W} = [w_1,\, w_2,\, w_3,\, w_4]^T \in \mathbb{R}^4 \to [w_1,\, w_2,\, w_3]$. Therefore $\mathbf{U}_i^{n+1}$ represents the discrete approximation of the relaxation Riemann solver without the component $\rho\,\Pi$. Then, the Godunov solver can be derived easily and reads:

$$\begin{aligned} \mathbf{U}_i^{n+1} &= \mathbf{U}_i^n - \frac{\Delta t}{\Delta x} \left(\mathbf{H}_{i+1/2}^n - \mathbf{H}_{i-1/2}^n \right) \\ \text{with: } \mathbf{H}_{i+1/2}^n &= L\left(\mathbf{F}^\mu \left(\mathbf{W}^{God}(0;\, \mathbf{W}_i^n,\, \mathbf{W}_{i+1}^n) \right) \right) = \mathbf{H}_{i+1/2}^n\,(\mathbf{U}_i^n,\, \mathbf{U}_{i+1}^n) \end{aligned} \tag{42}$$

The study of $\mathcal{C}^\mu$ and $\mathcal{A}^\mu$ leading to the explicit expression of the Godunov flux has been done in non-conservative variables $\mathbf{Z}^T = [\rho,\, u,\, \Pi,\, e]^T$. In the following, the structure of the fields, the eigenvalues and the Riemann invariants are described.

4.2.1 Convective Part

The relaxation system $\mathcal{C}^\mu$ is strictly hyperbolic, its eigenvalues being: $\lambda_1^{\mathcal{C},\mu} = u - \mathscr{E}_0\, a_{\mathcal{C}}\tau$, $\lambda_2^{\mathcal{C},\mu} = \lambda_3^{\mathcal{C},\mu} = u$, $\lambda_4^{\mathcal{C},\mu} = u + \mathscr{E}_0\, a_{\mathcal{C}}\tau$ with $\tau = 1/\rho$. Furthermore, each field is linearly degenerate and admits simple Riemann invariants:

$$\begin{aligned} \mathcal{I}^{\mathcal{C},\mu}_{\mathscr{E}_0,1} &= \left\{ u - \mathscr{E}_0\, a_{\mathcal{C}}\tau,\ \Pi + a_{\mathcal{C}}^2\tau,\ e + \frac{\mathscr{E}_0}{a_{\mathcal{C}}}\,\Pi\, u \right\} \\ \mathcal{I}^{\mathcal{C},\mu}_{\mathscr{E}_0,2,3} &= \{u,\ \Pi\} \\ \mathcal{I}^{\mathcal{C},\mu}_{\mathscr{E}_0,4} &= \left\{ u + \mathscr{E}_0\, a_{\mathcal{C}}\tau,\ \Pi + a_{\mathcal{C}}^2\tau,\ e - \frac{\mathscr{E}_0}{a_{\mathcal{C}}}\,\Pi\, u \right\} \end{aligned} \tag{43}$$

Let us notice that, for smooth solutions, mass equation in subsystem $\mathcal{C}^\mu$ can be rewritten $\partial_t\,\tau + u\,\partial_x\,\tau - \tau\,\partial_x\,u = 0$. By multiplying this equation by $a_{\mathcal{C}}^2$ and summing it with the Π equation in (36), one obtains:

$$\partial_t \left(\Pi + a_{\mathcal{C}}^2 \tau\right) + u\, \partial_x \left(\Pi + a_{\mathcal{C}}^2 \tau\right) = 0 \tag{44}$$

Thus, $\Pi + a_{\mathcal{C}}^2 \tau$ remains constant along the characteristic curves of speed u. Besides, it is a 2,3-strong Riemann invariant meaning that it is invariant through the 1-wave and the 4-wave. Eventually one can notice that this quantity is solution of the following equation:

$$\partial_\rho \left(\psi\right)_{|\Pi} + \left(\frac{a_{\mathcal{C}}}{\rho}\right)^2 \partial_\Pi \left(\psi\right)_{|\rho} = 0 \tag{45}$$

which can be related to the entropy equation (3). Pressure term linearization induced by the relaxation method has logically implied a linearization of the equation originally verified by entropy and $\Pi + a_{\mathcal{C}}^2 \tau$ seems to play the same role.

Beside, the knowledge of the Riemann invariants allow to easily solve the one-dimensional Riemann problem at a given face f, with $\mathbf{Z}_L$ and $\mathbf{Z}_R$ taken as initial conditions. Figure 1 describes the different states and waves produced:

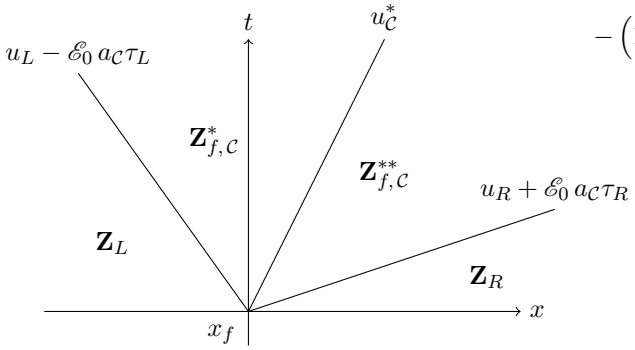

Figure 1: Subsystem $\mathcal{C}^\mu$: waves and states

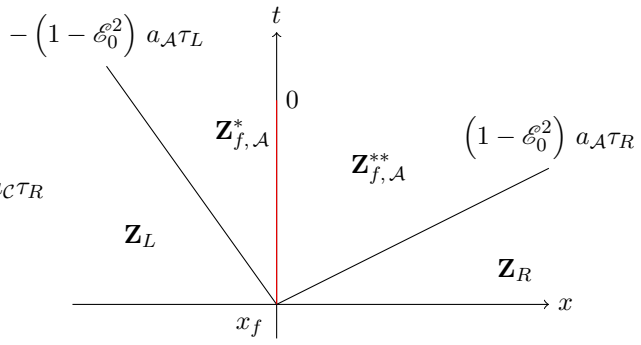

Figure 2: Subsystem $\mathcal{A}^\mu$: waves and states

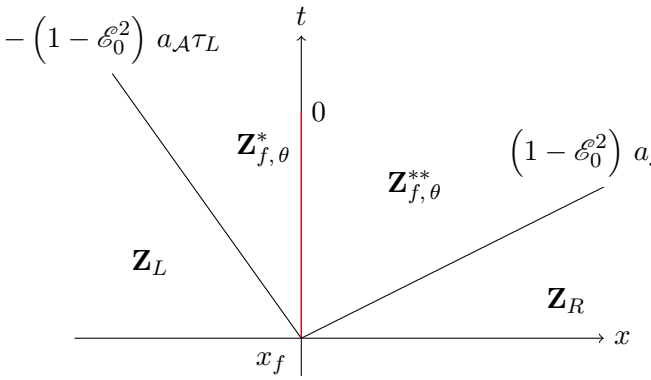

Figure 3: Approximate Riemann Solver of Subsystem $\mathcal{A}^\mu$: waves and states

The two intermediate states $\mathbf{Z}^*_{f,\mathcal{C}}$ and $\mathbf{Z}^{**}_{f,\mathcal{C}}$ are:

$$\mathbf{Z}^*_{f,\mathcal{C}} = \begin{bmatrix} \rho^*_{L,\mathcal{C}} \\ u^*_{\mathcal{C}} \\ \Pi^*_{\mathcal{C}} \\ e^*_{L,\mathcal{C}} \end{bmatrix} \quad \mathbf{Z}^{**}_{f,\mathcal{C}} = \begin{bmatrix} \rho^*_{R,\mathcal{C}} \\ u^*_{\mathcal{C}} \\ \Pi^*_{\mathcal{C}} \\ e^*_{R,\mathcal{C}} \end{bmatrix} \quad (46) \text{ with: } \begin{cases} u^*_{\mathcal{C}} = \dfrac{u_R + u_L}{2} - \dfrac{\mathscr{E}_0}{2\, a_{\mathcal{C}}} (p_R - p_L) \\ \mathscr{E}_0^2\, \Pi^*_{\mathcal{C}} = \mathscr{E}_0^2\, \dfrac{p_R + p_L}{2} - \dfrac{\mathscr{E}_0\, a_{\mathcal{C}}}{2} (u_R - u_L) \\ \rho^*_{k,\mathcal{C}} = 1/\tau^*_{k,\mathcal{C}},\ \tau^*_{k,\mathcal{C}} = \tau_k + \dfrac{(-1)^{i_k+1}}{\mathscr{E}_0\, a_{\mathcal{C}}} (u^*_{\mathcal{C}} - u_k) \\ e^*_{k,\mathcal{C}} = e_k + \mathscr{E}_0\, \dfrac{(-1)^{i_k}}{a_{\mathcal{C}}} (\Pi^*_{\mathcal{C}}\, u^*_{\mathcal{C}} - p_k\, u_k) \\ k \in \{L,\, R\},\ i_L = 1,\ i_R = 2 \end{cases} \quad (47)$$

Remark 6. *In* (47)*, one can observe that the non-centered terms of the intermediate velocity and the intermediate pressure flux are systematically multiplied by the weighting parameter* $\mathscr{E}_0$*. In* ***Section 5****, it will be shown that this dependence has a strong impact in the numerical diffusion reduction in the case of a low-Mach number flow.*

Define $\mathbf{W}^{*,n}_{i+1/2}$ (respectively $\mathbf{W}^{**,n}_{i+1/2}$) using $\mathbf{Z}^*_{i+1/2,\mathcal{C}}$ (respectively $\mathbf{Z}^{**}_{i+1/2,\mathcal{C}}$) and introduce $\mathbf{U}^{*,n}_{i+1/2} = L\left(\mathbf{W}^{*,n}_{i+1/2}\right)$, $\mathbf{U}^{**,n}_{i+1/2} = L\left(\mathbf{W}^{**,n}_{i+1/2}\right)$. The convective numerical flux then reads:

$$\mathbf{H}_{\mathbf{c}}{}^n_{i+1/2} = \begin{cases} L\left(\mathbf{F}^{\mu}_{\mathcal{C}}\right)\left(\mathbf{U}^n_i\right) & \text{if } u^n_i - \mathscr{E}^n_0\, (a^n_{\mathcal{C}})_{i+1/2} \tau^n_i > 0 \\ L\left(\mathbf{F}^{\mu}_{\mathcal{C}}\right)\left(\mathbf{U}^{*,n}_{i+1/2}\right) & \text{if } u^n_i - \mathscr{E}^n_0\, (a^n_{\mathcal{C}})_{i+1/2} \tau^n_i \leq 0 < (u^*_{\mathcal{C}})^n_{i+1/2} \\ L\left(\mathbf{F}^{\mu}_{\mathcal{C}}\right)\left(\mathbf{U}^{**,n}_{i+1/2}\right) & \text{if } (u^*_{\mathcal{C}})^n_{i+1/2} \leq 0 < u^n_{i+1} + \mathscr{E}^n_0\, (a^n_{\mathcal{C}})_{i+1/2} \tau^n_{i+1} \\ L\left(\mathbf{F}^{\mu}_{\mathcal{C}}\right)\left(\mathbf{U}^n_{i+1}\right) & \text{if } u^n_{i+1} + \mathscr{E}^n_0\, (a^n_{\mathcal{C}})_{i+1/2} \tau^n_{i+1} \leq 0 \\ (a^n_{\mathcal{C}})_{i+1/2} = & K\, max\left(\rho^n_i\, (c_{\mathcal{C}})^n_i,\, \rho^n_{i+1}\, (c_{\mathcal{C}})^n_{i+1}\right),\ K > 1 \end{cases} \quad (48)$$

Furthermore, using the exact Godunov structure and the fact that all the fields are linearly degenerate, one can rewrite the relaxation flux in a more compact way (see [2, 3]) as:

$$\mathbf{H}_{\mathbf{c}}{}^n_{i+1/2} = \begin{cases} \dfrac{1}{2}\left(L\left(\mathbf{F}^{\mu}_{\mathcal{C}}\right)\left(\mathbf{U}^n_i\right) + L\left(\mathbf{F}^{\mu}_{\mathcal{C}}\right)\left(\mathbf{U}^n_{i+1}\right)\right) \\ -\dfrac{1}{2}\left|u^n_i - \mathscr{E}^n_0\, (a^n_{\mathcal{C}})_{i+1/2}\, \tau^n_i\right| \left(\mathbf{U}^{*,n}_{i+1/2} - \mathbf{U}^n_i\right) \\ -\dfrac{1}{2}\left|(u^*_{\mathcal{C}})^n_{i+1/2}\right| \left(\mathbf{U}^{**,n}_{i+1/2} - \mathbf{U}^{*,n}_{i+1/2}\right) \\ -\dfrac{1}{2}\left|u^n_{i+1} + \mathscr{E}^n_0\, (a^n_{\mathcal{C}})_{i+1/2}\, \tau^n_{i+1}\right| \left(\mathbf{U}^n_{i+1} - \mathbf{U}^{**,n}_{i+1/2}\right) \end{cases} \quad (49)$$

4.2.2 Acoustic Part

The acoustic system $\mathcal{A}^{\mu}$ is also hyperbolic and its eigenvalues are: $\lambda_1^{\mathcal{A},\mu} = -(1 - \mathscr{E}_0^2)\, a_{\mathcal{A}}\tau$, $\lambda_2^{\mathcal{A},\mu} = \lambda_3^{\mathcal{A},\mu} = 0$, $\lambda_4^{\mathcal{A},\mu} = (1 - \mathscr{E}_0^2)\, a_{\mathcal{A}}\tau$. Once again the Riemann invariants can

be easily found and read:

$$\begin{aligned}
\mathcal{I}^{\mathcal{A},\mu}_{\mathscr{E}_0,1} &= \left\{\rho,\ u+\frac{\Pi}{a_{\mathcal{A}}},\ e+\frac{\Pi\,u}{a_{\mathcal{A}}}\right\}\\
\mathcal{I}^{\mathcal{A},\mu}_{\mathscr{E}_0,2,3} &= \{u,\ \Pi\}\\
\mathcal{I}^{\mathcal{A},\mu}_{\mathscr{E}_0,4} &= \left\{\rho,\ u-\frac{\Pi}{a_{\mathcal{A}}},\ e-\frac{\Pi\,u}{a_{\mathcal{A}}}\right\}
\end{aligned} \tag{50}$$

It can be noticed that:

$$\begin{aligned}
\partial_t\left(u+\frac{\Pi}{a_{\mathcal{A}}}\right)+\lambda_4^{\mathcal{A},\mu}\,\partial_x\left(u+\frac{\Pi}{a_{\mathcal{A}}}\right)=0\\
\partial_t\left(u-\frac{\Pi}{a_{\mathcal{A}}}\right)+\lambda_1^{\mathcal{A},\mu}\,\partial_x\left(u-\frac{\Pi}{a_{\mathcal{A}}}\right)=0
\end{aligned} \tag{51}$$

Thus, $\omega^+_{\mathcal{A}}=u+\dfrac{\Pi}{a_{\mathcal{A}}}$ (respectively $\omega^-_{\mathcal{A}}=u-\dfrac{\Pi}{a_{\mathcal{A}}}$) remains constant along the characteristic curves of speed $\lambda_4^{\mathcal{A},\mu}$ (respectively $\lambda_1^{\mathcal{A},\mu}$). Besides, $\omega^+_{\mathcal{A}}$ is a 4-strong Riemann invariant whereas $\omega^-_{\mathcal{A}}$ is a 1-strong Riemann invariant. Following the steps of [13] and [22], equations (51) associated with the strong Riemann invariants natural properties provides a simple way to derive a time-implicit relaxation scheme for the acoustic subsystem. More details will be given in [28, 29].

The one-dimensional Riemann problem can be solved exactly without difficulty. The solution is described on Figure 2.

$$\mathbf{Z}^*_{f,\mathcal{A}}=\begin{bmatrix}\rho_L\\ u^*_{\mathcal{A}}\\ \Pi^*_{\mathcal{A}}\\ e^*_{L,\mathcal{A}}\end{bmatrix}\quad \mathbf{Z}^{**}_{f,\mathcal{A}}=\begin{bmatrix}\rho_R\\ u^*_{\mathcal{A}}\\ \Pi^*_{\mathcal{A}}\\ e^*_{R,\mathcal{A}}\end{bmatrix} \tag{52}$$

with:

$$\begin{cases}
u^*_{\mathcal{A}}=\dfrac{u_R+u_L}{2}-\dfrac{1}{2\,a_{\mathcal{A}}}\,(p_R-p_L)\\
\Pi^*_{\mathcal{A}}=\dfrac{p_R+p_L}{2}-\dfrac{a_{\mathcal{A}}}{2}\,(u_R-u_L)\\
e^*_{k,\mathcal{A}}=e_k+\dfrac{(-1)^{i_k}}{a_{\mathcal{A}}}\,(\Pi^*_{\mathcal{A}}\,u^*_{\mathcal{A}}-p_k\,u_k)\\
k\in\{L,\,R\}\,,\ i_L=1,\ i_R=2
\end{cases} \tag{53}$$

One can notice that the weighting parameter $\mathscr{E}_0$ does not appear in the different intermediate quantities. Besides, the intermediate velocity, pressure and energy formulas are similar to those obtained using the Lagrange-Projection method [22, 8]. The only difference is that, in the present approach, $a_{\mathcal{A}}$ is bounded by the modified acoustic subcharacteristic condition (37b) whereas in [22, 8] it is (39). The related numerical flux writes:

$$\begin{aligned}
\mathbf{H_{ac}}^{\,n}_{i+1/2} &= \left(1-(\mathscr{E}_0^n)^2\right)\begin{bmatrix}0\\ (\Pi^*_{\mathcal{A}})^n_{i+1/2}\\ (\Pi^*_{\mathcal{A}})^n_{i+1/2}\,(u^*_{\mathcal{A}})^n_{i+1/2}\end{bmatrix}\\
(a^n_{\mathcal{A}})_{i+1/2} &= K\,max\left(\rho^n_i\,(c_{\mathcal{A}})^n_i,\,\rho^n_{i+1}\,(c_{\mathcal{A}})^n_{i+1}\right),\ K>1
\end{aligned} \tag{54}$$

4.2.3 General Remarks on the Splitting Operator Algorithm:

The overall algorithm to update the discrete solution from t^n to $t^n + \Delta t$ is the following: starting from a given state $\mathbf{U}^n$, a given relaxation pressure $\Pi^n = p^{EOS}(\mathbf{U}^n)$ and a given splitting parameter $\mathscr{E}_0^n$, subsystems $\mathcal{C}^\mu$ and $\mathcal{A}^\mu$ are successively solved using the relaxation scheme fluxes presented in (48) and (54). Note that in each resolution step, the relaxation right hand side "$(p-\Pi)/\mu$" is immediately taken into account by supposing that the equilibrium timescale is zero. In the formalism of [4], it corresponds to the solution projection of the relaxation Riemann problem on the Maxwellian equilibrium. Afterwards, the weighting factor $\mathscr{E}_0$ is updated. One can notice that the overall operator splitting procedure is conservative since $\mathcal{C}$ and $\mathcal{A}$ are conservative subsystems and the resolution of $\mathcal{C}^\mu$ and $\mathcal{A}^\mu$ is performed using an exact conservative Godunov scheme. The global relaxation scheme including both steps writes:

$$\begin{cases} \mathbf{U}_i^{n+} = \mathbf{U}_i^n - \dfrac{\Delta t}{\Delta x}\left(\mathbf{H}_{\mathbf{c}i+1/2}\left(\mathbf{U}_i^n,\, \mathbf{U}_{i+1}^n\right) - \mathbf{H}_{\mathbf{c}i-1/2}\left(\mathbf{U}_{i-1}^n,\, \mathbf{U}_i^n\right)\right), \\ \mathbf{\Pi}_i^{n+} = p^{EOS}\left(\mathbf{U}_i^{n+}\right), \end{cases}$$
$$\begin{cases} \mathbf{U}_i^{n+1} = \mathbf{U}_i^{n+} - \dfrac{\Delta t}{\Delta x}\left(\mathbf{H}_{\mathbf{ac}i+1/2}\left(\mathbf{U}_i^{n+},\, \mathbf{U}_{i+1}^{n+}\right) - \mathbf{H}_{\mathbf{ac}i-1/2}\left(\mathbf{U}_{i-1}^{n+},\, \mathbf{U}_i^{n+}\right)\right), \\ \mathbf{\Pi}_i^{n+1} = p^{EOS}\left(\mathbf{U}_i^{n+1}\right). \end{cases} \tag{55}$$

Written in one single conservative step, the scheme reads:

$$\begin{aligned} \mathbf{U}_i^{n+1} = \mathbf{U}_i^n &- \frac{\Delta t}{\Delta x}\left(\mathbf{H}_{\mathbf{c}i+1/2}\left(\mathbf{U}_i^n,\, \mathbf{U}_{i+1}\right) - \mathbf{H}_{\mathbf{c}i-1/2}^n\left(\mathbf{U}_{i-1}^n,\, \mathbf{U}_i^n\right)\right), \\ &- \frac{\Delta t}{\Delta x}\left(\mathbf{H}_{\mathbf{ac}i+1/2}\left(\mathbf{U}_i^{n+},\, \mathbf{U}_{i+1}^{n+}\right) - \mathbf{H}_{\mathbf{ac}i-1/2}\left(\mathbf{U}_{i-1}^{n+},\, \mathbf{U}_i^{n+}\right)\right). \end{aligned} \tag{56}$$

So far the time-dependent weighting factor $\mathscr{E}_0^n$ has not been defined exactly. However, following the insights of **Subsection 2.2**, one can define:

$$\begin{aligned} \mathscr{E}_0^n &= \max\left(\mathscr{E}_{inf},\, \min\left((M_{max}^n)^\alpha,\, 1\right)\right) \\ \text{with: } M_{max}^n &= \max_{i\in[1,\, N_{cells}]}\left(\frac{|u_i^n|}{c_i^n}\right) \end{aligned} \tag{57}$$

Here, $c_i^n = c\left(\rho_i^n,\, p_i^n\right)$ where $c(.,.)$ is the sound speed function defined in equation (1e). α is a positive power which will be determined in **Section 5**. Eventually, $0 < \mathscr{E}_{inf} \ll 1$ is only a lower bound preventing $\mathscr{E}_0^n$ from being exactly equal to zero if velocity is initially null everywhere.

4.3 CFL Condition Choice

Definition 1 (CFL condition based on the Euler system)**.** In order to adapt timesteps to the real waves produced by the Euler system, let us define the discrete time step at

iteration n as:

$$\Delta t_E^n = \frac{\sigma}{2} \frac{\Delta x}{\underset{i+1/2}{max} \left(max \left(|u_i^n| + c_i^n,\, \left| u_{i+1}^n \right| + c_{i+1}^n \right) \right)}, \qquad (58)$$
$$0 < \sigma < 1.$$

CFL condition (58) is adapted to the resolution of the overall Euler system. However, because of the weighted splitting approach, one can exhibit two additional CFL conditions which would be sufficient to guarantee stability of both $\mathcal{C}$ and $\mathcal{A}$ subsystems if they were solved independently. These CFL conditions write:

$$\Delta t_{\mathcal{C}}^n = \frac{\sigma}{2} \frac{\Delta x}{\underset{i+1/2}{max} \left(max \left(\left| u_i^n - \mathscr{C}_0^n \left(a_{\mathcal{C}} \right)_{i+1/2}^n \tau_i^n \right|,\, \left| u_{i+1}^n + \mathscr{C}_0^n \left(a_{\mathcal{C}} \right)_{i+1/2}^n \tau_{i+1}^n \right| \right) \right)},$$
$$\Delta t_{\mathcal{A}}^n = \frac{\sigma}{2} \frac{\Delta x}{(1 - (\mathscr{C}_0^n)^2) \underset{i+1/2}{max} \left(\left(a_{\mathcal{A}} \right)_{i+1/2}^n max \left(\tau_i^n,\, \tau_{i+1}^n \right) \right)}, \qquad (59)$$
$$0 < \sigma < 1.$$

One should keep in mind that it is absolutely not sufficient, in a fractional-step method, to constrain the timestep by only substeps CFL condition in order to guarantee the stability of the overall algorithm. A very simple hand-made but rather convincing example described in [14] shows that the CFL condition of the unsplit system has to be taken into account too. Hence, the final CFL condition reads:

$$\Delta t^n = min \left(\Delta t_E^n,\, \Delta t_{\mathcal{C}}^n,\, \Delta t_{\mathcal{A}}^n \right). \qquad (60)$$

We now study the discrete properties of our weighted splitting approach. Special attention will be held on positivity of both density and internal energy.

4.4 Discrete Properties of the Overall Scheme

4.4.1 Discrete Density Positivity

Let us first notice that the acoustic resolution step of $\mathcal{A}^\mu$ does not modify density. Then, one has just to check that discrete density remains positive after the convective step. This is classically done in [2] by rewriting the convective relaxation scheme (42), (48) as:

$$\mathbf{U}_i^{n+1} = \frac{\mathbf{U}^+ \left(\mathbf{W}_i^n,\, \mathbf{W}_{i-1}^n \right) + \mathbf{U}^- \left(\mathbf{W}_{i+1}^n,\, \mathbf{W}_i^n \right)}{2}$$
$$\text{with: } \mathbf{U}^+ \left(\mathbf{W}_L,\, \mathbf{W}_R \right) = \frac{2\,\Delta t}{\Delta x} \int_0^{\frac{\Delta x}{2\,\Delta t}} L \left(\mathbf{W}^{God} \right) \left(\xi,\, \mathbf{W}_L,\, \mathbf{W}_R \right) d\,\xi \qquad (61)$$
$$\mathbf{U}^- \left(\mathbf{W}_L,\, \mathbf{W}_R \right) = \frac{2\,\Delta t}{\Delta x} \int_{-\frac{\Delta x}{2\,\Delta t}}^0 L \left(\mathbf{W}^{God} \right) \left(\xi,\, \mathbf{W}_L,\, \mathbf{W}_R \right) d\,\xi$$

Hence, positivity of the discrete density ρ_i^{n+1} is maintained if all the intermediate densities appearing in the Riemann problem described on Figure 1 and equalities (47) are

positive. This can be done by adding an additional lower bound for constant $a_{\mathcal{C}}$ into the subcharacteristic condition (37a):

Lemma 1 (Positivity of intermediate density)**.** *Consider the Riemann problem related to subsystem $\mathcal{C}$, producing waves described on Figure 1 with $\mathbf{U}_L$ and $\mathbf{U}_R$ as initial data. Assume that the global CFL condition* (60) *holds and that the initial data are such that:*

$$-\frac{\rho_L\,(u_R-u_L)^2}{8} \leq \mathscr{E}_0^2\,(p_R-p_L) \leq \frac{\rho_R\,(u_R-u_L)^2}{8}, \tag{62}$$

then, the intermediate densities $\rho^*_{L,\mathcal{C}}$ and $\rho^*_{R,\mathcal{C}}$ defined in (47) *are positive under the modified subcharacteristic condition:*

$$\mathcal{C}^\mu:\ a_{\mathcal{C}} \geq max\left(\rho_L\,(c_{\mathcal{C}})_L,\,\rho_R\,(c_{\mathcal{C}})_R,\,a_L^\rho,\,a_R^\rho\right), \tag{63}$$

with:

$$\begin{aligned} a_L^\rho &= \frac{1}{2}\left(-\frac{\rho_L\,(u_R-u_L)}{2\,\mathscr{E}_0}+\sqrt{\frac{\rho_L^2\,(u_R-u_L)^2}{4\,\mathscr{E}_0^2}+2\,\rho_L\,(p_R-p_L)}\right),\\ a_R^\rho &= \frac{1}{2}\left(-\frac{\rho_R\,(u_R-u_L)}{2\,\mathscr{E}_0}+\sqrt{\frac{\rho_R^2\,(u_R-u_L)^2}{4\,\mathscr{E}_0^2}-2\,\rho_R\,(p_R-p_L)}\right). \end{aligned} \tag{64}$$

Furthermore, if the first (respectively the second) inequality in (62) *does no longer hold, a_L^ρ (respectively a_R^ρ) can be removed from* (63)*. Eventually, it is equivalent to guarantee the intermediate density positivity and the ordering of the waves speeds: $u_L-\mathscr{E}_0\,a_{\mathcal{C}}\,\tau_L \leq u^*_{\mathcal{C}} \leq u_R+\mathscr{E}_0\,a_{\mathcal{C}}\,\tau_R$.*

The proof of this lemma is written in Appendix C. The same kind of results can be found in [2] in order to enforce the mass fraction positivity. One can notice that the non dimensional expressions of a_L^ρ and a_R^ρ are of order $O(1+M/\mathscr{E}_0)$. The order one term is inherited from the pressure difference under the square root while $(u_R-u_L)/\mathscr{E}_0$ provides the order $O(M/\mathscr{E}_0)$ term. Therefore, in order to make sure that a_L^ρ and a_R^ρ remain of order one one could impose $\alpha \geq 1$ in the definition of $\mathscr{E}_0$ (8).

4.4.2 Discrete Internal Energy Positivity

As already presented in **Subsection 2.2.2**, in the case of an ideal gas thermodynamics, specific internal energy ε remains positive throughout space and time. Although ε is not a conservative variable, we can still consider equation (61) seen as a continuous convex combination of conservative states and notice that Φ_{PG} defined in (13) is a convex set in the conservative phase-space. Thus, similarly to density, a sufficient condition to guarantee the positivity of ε^{n+1} is to make sure that for $k \in \{L,\,R\}$, $\varepsilon^*_{k,\mathcal{C}} = e^*_{k,\mathcal{C}} - (u^*_{\mathcal{C}})^2/2$ as well as $\varepsilon^*_{k,\mathcal{A}} = e^*_{k,\mathcal{A}} - (u^*_{\mathcal{A}})^2/2$ are positive. Such a sufficient condition is presented in the next lemma:

Lemma 2 (Positivity of the intermediate internal energy)**.** *Consider the Riemann problem related to subsystems $\mathcal{C}$ and $\mathcal{A}$, producing waves described on Figure 1 and Figure 2 with*

$\mathbf{U}_L$ *and* $\mathbf{U}_R$ *as initial data. Assume that the global CFL condition* (60) *holds and that the initial data are such that:*

$$\begin{aligned} &max\left(-\frac{\rho_L\,(u_R-u_L)^2}{8},\,-\frac{\mathscr{E}_0^2\,\rho_R^\varepsilon\,(u_R-u_L)^2}{8}\right)\leq \mathscr{E}_0^2\,(p_R-p_L)\leq min\left(\frac{\rho_R\,(u_R-u_L)^2}{8},\,\frac{\mathscr{E}_0^2\,\rho_L^\varepsilon\,(u_R-u_L)^2}{8}\right),\\ &\text{with: } \rho_k^\varepsilon=p_k/\varepsilon_k,\ k\in\{L,\,R\}\,. \end{aligned} \tag{65}$$

then, the intermediate internal energies $\varepsilon^*_{k,\mathcal{C}}$ *and* $\varepsilon^*_{k,\mathcal{A}}$, $k\in\{L,\,R\}$ *defined above are positive under the modified subcharacteristic conditions:*

$$\begin{aligned} &\mathcal{C}^\mu:\ a_{\mathcal{C}}\geq max\left(\rho_L\,(c_{\mathcal{C}})_L,\,\rho_R\,(c_{\mathcal{C}})_R,\,a_L^\rho,\,a_R^\rho,\,a_L^\varepsilon,\,a_R^\varepsilon\right),\\ &\mathcal{A}^\mu:\ a_{\mathcal{A}}\geq max\left(\rho_L\,(c_{\mathcal{A}})_L,\,\rho_R\,(c_{\mathcal{A}})_R,\,a_L^\varepsilon,\,a_R^\varepsilon\right), \end{aligned} \tag{66}$$

with:

$$\begin{aligned} a_L^\varepsilon&=\frac{1}{2}\left(-\frac{\rho_L^\varepsilon\,(u_R-u_L)}{2\,\mathscr{E}_0}+\sqrt{\frac{\left(\rho_R^\varepsilon\,(u_R-u_L)\right)^2}{4\,\mathscr{E}_0^2}-2\,\rho_L^\varepsilon\,(p_R-p_L)}\right),\\ a_R^\varepsilon&=\frac{1}{2}\left(-\frac{\rho_R^\varepsilon\,(u_R-u_L)}{2\,\mathscr{E}_0}+\sqrt{\frac{\left(\rho_R^\varepsilon\,(u_R-u_L)\right)^2}{4\,\mathscr{E}_0^2}+2\,\rho_R^\varepsilon\,(p_R-p_L)}\right). \end{aligned} \tag{67}$$

Furthermore, as for ***Lemma1****, if any of the inequalities* (65) *does not hold, it allows to remove either* a_k^ρ *or* a_k^ε *(according to the case) from* (66)*.*

The proof of this lemma is written in Appendix D. Once again, if $\alpha\geq 1$ in the definition of $\mathscr{E}_0$, the non-dimensional expressions of a_k^ε are of order one.

In the following section, a truncation error analysis performed on smooth solutions is derived in order to exactly determine the power α.

5 A Truncation Error Analysis to Fit $\mathscr{E}_0^2(t)$

As studied in [22, 8] and mentioned in **Subsection 2.2**, most of low-Mach flows issues result in substantial non-dimensional spatial diffusion at discrete level, the order of the diffusion coefficient being $O(\Delta x/M)$. That is why, in this section, we are interested in performing a truncation error analysis on the convective, the acoustic and the overall relaxation schemes. This will allow us to determine how our weighting parameter $\mathscr{E}_0$ should be designed in order to tackle the numerical diffusion in the case of low-Mach flows.

5.1 Truncation Error of the Weighted Splitting Subsystems

Here is the truncation error analysis performed on the convective subsystem $\mathcal{C}$:

Proposition 2 (Truncation error analysis of the convective subsystem)**.** *Consider the convective numerical scheme defined by equations* (42)*,* (48) *and* (49)*. Under the CFL condition* (58)*, This scheme is consistent with the non-dimensional convective subsystem:*

$$\mathcal{C}^{trunc}: \begin{cases} \partial_t \rho + \partial_x (\rho u) = O(M\Delta x) + O\left((1 + \dfrac{\mathscr{E}_0}{M} + \dfrac{M}{\mathscr{E}_0})\Delta x\right), \\ \partial_t (\rho u) + \partial_x \left(\rho u^2 + \dfrac{\mathscr{E}_0^2(t)}{M^2} p\right) = O(M\Delta x) + O\left((1 + \dfrac{\mathscr{E}_0}{M} + \dfrac{M}{\mathscr{E}_0})\Delta x\right), \\ \partial_t (\rho e) + \partial_x \left((\rho e + \mathscr{E}_0^2(t)\, p)\, u\right) = O(M\Delta x) + O\left((1 + \dfrac{\mathscr{E}_0}{M} + \dfrac{M}{\mathscr{E}_0})\Delta x\right). \end{cases} \tag{68}$$

The proof is given in Appendix G. As previously announced in **Remark 6**, the factor $\mathscr{E}_0$ in front of the non-centered terms of the intermediate velocity and pressure flux defined in (47) naturally compensates the $1/M$ terms of the non-dimensional diffusive operator. Thus, considering that there is a smooth function $t \to \mathscr{E}_0(t)$ such as $\mathscr{E}_0(t^n) = \mathscr{E}_0^n$, with $\mathscr{E}_0^n$ defined in (57), one can notice that:

$$O\left(\frac{M}{\mathscr{E}_0}\right) = O\left(\frac{\mathscr{E}_0}{M}\right) = O(1) \Leftrightarrow \alpha = 1 \text{ in (57)}. \tag{69}$$

Therefore, by re-defining

$$\begin{aligned} \mathscr{E}_0^n &= \max\left(\mathscr{E}_{inf},\, \min\left(M_{max}^n,\, 1\right)\right), \\ \text{with: } M_{max}^n &= \underset{i \in [1,\, N_{cells}]}{max} \left(\frac{u_i^n}{c_i^n}\right), \end{aligned} \tag{70}$$

the numerical diffusion produced by the convective subsystem $\mathcal{C}$ is of order $O(\Delta x)$ in every Mach regime. If the convective part of the present weighted splitting approach structurally avoids low-Mach numerical diffusion, the acoustic one continues to suffer from it. Indeed:

Proposition 3 (Truncation error analysis of the acoustic subsystem)**.** *Consider the acoustic numerical scheme defined by equations* (42) *and* (54)*. Under the CFL condition* (58)*, This scheme is consistent with the non-dimensional acoustic subsystem:*

$$\mathcal{A}^{trunc}: \begin{cases} \partial_t \rho = O(M\Delta x), \\ \partial_t (\rho u) + \partial_x \left(\dfrac{(1 - \mathscr{E}_0^2(t))}{M^2} p\right) = O(M\Delta x) + O\left(\dfrac{(1 - \mathscr{E}_0^2)}{M} \Delta x\right), \\ \partial_t (\rho e) + \partial_x \left((1 - \mathscr{E}_0^2(t))\, p\, u\right) = O(M\Delta x) + O\left((1 - \mathscr{E}_0^2)(M + \dfrac{1}{M})\Delta x\right). \end{cases} \tag{71}$$

As it can be seen in the momentum equation (71), the order $1/M$ terms of the correction part of the flux are solely weighted by $(1 - \mathscr{E}_0^2)$. What is more, as noted in Appendix G, the overall relaxation scheme suffers from an additional numerical diffusion of order $\dfrac{(1 - \mathscr{E}_0^2)\Delta x}{M}$. Indeed, after the convective step, and under the CFL condition (58), it can be shown that a smooth non-dimensional updated solution $\mathbf{U}_i^{n+}$ is such that:

$$
\begin{aligned}
&\mathbf{U}_i^{n+} = \mathbf{U}_i^n + \mathbf{B}_i^n M\Delta x + \underline{O}\left(M(1+\frac{\mathscr{E}_0}{M}+\frac{M}{\mathscr{E}_0})\Delta x^2\right),\\
&\text{with: } \mathbf{B}_i^n = -\partial_x\ L\left(\mathbf{F}_{\mathcal{C}}^{\mu}\right)\left(\mathbf{U}_i^n\right)\ A^n,\\
&\text{with: } A^n = \frac{\sigma}{\underset{i+1/2}{max}\left(|u_i^n|+c_i^n,\ \left|u_{i+1}^n\right|+c_{i+1}^n\right)},\ 0<\sigma<1.
\end{aligned}
\tag{72}
$$

Then, if no additional hypothesis is done on the initial input $\mathbf{U}_i^n$, $\mathbf{B}_i^n$ is of order one a priori. Injected inside the centered pressure part of the acoustic momentum flux, the fluctuation generated by the convective step entails a new diffusion term of order $\dfrac{(1-\mathscr{E}_0^2)\Delta x}{M}$. However if the initial input lies into the discrete well-prepared space:

$$
\begin{aligned}
&\rho_i^n = \rho_0 + O\left(M\right),\\
&u_i^n = u_0 + O\left(M\right),\\
&p_i^n = p_0 + O\left(M^2\right),\\
&\text{with: } \rho_0,\ u_0,\ p_0 \text{ constants of order one,}
\end{aligned}
\tag{73}
$$

then $\mathbf{B}_i^n$ becomes of order M and the dependence in $1/M$ of the new diffusive term vanishes.

In any case, a last special treatment has to be implemented to remove the $O\left(\dfrac{(1-\mathscr{E}_0^2)\Delta x}{M}\right)$ diffusive terms brought by the acoustic correction part in the momentum flux.

5.2 Low-Mach Correction of the Acoustic Splitting Step

The low-Mach correction inspired from [17, 22] consists in adding artificially a term of order $O(M)$ in front of the correction part in the acoustic momentum flux. This new term can be built using the local velocity and sound speed. The modified acoustic flux reads:

$$
\begin{aligned}
&{\mathbf{H}_{\mathbf{ac}}}_{i+1/2}^n = \left(1-(\mathscr{E}_0^n)^2\right)\begin{bmatrix}0\\(\Pi^*_{\mathcal{A},\,\theta})_{i+1/2}^n\\(\Pi^*_{\mathcal{A},\,\theta}\,u^*_{\mathcal{A}})_{i+1/2}^n\end{bmatrix},\\
&\text{with: } (\Pi^*_{\mathcal{A},\,\theta})_{i+1/2}^n = \frac{p_{i+1}^n+p_i^n}{2} - \frac{(a_{\mathcal{A}}\,\theta)_{i+1/2}^n}{2}\left(u_{i+1}^n-u_i^n\right),\\
&\text{and: } \theta_{i+1/2}^n = min\left(\frac{\left|(u_A^*)_{i+1/2}^n\right|}{max\left(c_{i+1}^n,\,c_i^n\right)},\,1\right).
\end{aligned}
\tag{74}
$$

As noticed in [22], the introduction of this low-Mach correction does not alter the consistency of the numerical scheme because it solely impacts the non-centered part in the momentum flux which is only responsible for the numerical diffusion. Furthermore, it is possible to build an approximate Riemann solver in the sense of Harten, Lax and Van Leer [27] with the same eigenvalues than those produced by the exact Riemann problem associated to the acoustic relaxation system $\mathcal{A}^{\mu}$. Details on this approximate Riemann

solver are given in Figure 3, and equations (75), (76). The insensitivity of the eigenvalues to the low-Mach correction allows to maintain the same kind of CFL condition (60) for the modified acoustic scheme.

$$\mathbf{Z}^*_{f,\theta} = \begin{bmatrix} \rho_L \\ u^*_{L,\theta} \\ \Pi^*_{\mathcal{A},\theta} \\ e^*_{L,\theta} \end{bmatrix}, \quad \mathbf{Z}^{**}_{f,\theta} = \begin{bmatrix} \rho_R \\ u^*_{R,\theta} \\ \Pi^*_{\mathcal{A},\theta} \\ e^*_{R,\theta} \end{bmatrix} \tag{75}$$

$$\text{with: } \begin{cases} u^*_{k,\theta} = u^*_{\mathcal{A}} + (-1)^{i_k}\,(1-\theta)\dfrac{(u_R - u_L)}{2}, \\ e^*_{k,\theta} = e^*_{k,\mathcal{A}} + (-1)^{i_k}\,(1-\theta)\dfrac{(u_R - u_L)\,u^*_{\mathcal{A}}}{2}, \\ \quad k \in \{L,\,R\}\,,\ i_L = 1,\ i_R = 2. \end{cases} \tag{76}$$

Thanks to this low-Mach correction term, numerical diffusion of the subsystem $\mathcal{A}$ is modified, namely:

Proposition 4 (Truncation error analysis of the acoustic subsystem with low-Mach correction)**.** *Consider the acoustic numerical scheme defined by equations* (42) *with the low-Mach corrected flux* (74)*. Suppose that pressure follows the well-prepared initial condition written in* (73)*. Then, under the CFL condition* (58)*, This scheme is consistent with the non-dimensional acoustic subsystem:*

$$\mathcal{A}^{trunc}: \begin{cases} \partial_t\,\rho = O(M\Delta x), \\ \partial_t\,(\rho\,u) + \partial_x\left(\dfrac{(1-\mathscr{E}_0^2(t))}{M^2}\,p\right) = O(M\Delta x) + O\left(\dfrac{(1-\mathscr{E}_0^2)\theta}{M}\Delta x\right), \\ \partial_t\,(\rho\,e) + \partial_x\left((1-\mathscr{E}_0^2(t))\,p\,u\right) = O(M\Delta x) + O\left((1-\mathscr{E}_0^2)(1+\theta)M\Delta x\right). \end{cases} \tag{77}$$

Assume that there exists a smooth function $(x,t) \to \theta(x,\,t)$ such that $\forall(i,\,n),\ \theta(x_{i+1/2},\,t^n) = \theta^n_{i+1/2}$. Then the numerical diffusion contained in the term of order $O\left(\dfrac{(1-\mathscr{E}_0^2)\theta}{M}\Delta x\right)$ is actually of order $O\left((1-\mathscr{E}_0^2)\Delta x\right)$. Moreover, the global truncation error analysis writes:

Proposition 5 (Truncation error analysis of the overall scheme with low-Mach correction)**.** *Consider the global relaxation scheme defined by equations* (56) *endowed with the low-Mach corrected acoustic flux* (74)*. Suppose that initial state* $\mathbf{U}_i^n$ *follows the well-prepared initial condition written in* (73)*. Then, under the CFL condition* (58)*, this scheme is consistent with the non-dimensional system:*

$$\mathcal{E}^{trunc}: \begin{cases} \partial_t\,\rho + \partial_x\,(\rho\,u) = O(M\Delta x) + O\left((1 + \dfrac{\mathscr{E}_0}{M} + \dfrac{M}{\mathscr{E}_0})\Delta x\right), \\ \partial_t\,(\rho\,u) + \partial_x\left(\rho\,u^2 + \dfrac{p}{M^2}\right) = O(M\Delta x) + O\left((1 + \dfrac{\mathscr{E}_0}{M} + \dfrac{M}{\mathscr{E}_0})\Delta x\right) \\ \qquad\qquad + O\left((1-\mathscr{E}_0^2)(1 + \dfrac{\theta}{M})\Delta x\right), \\ \partial_t\,(\rho\,e) + \partial_x\,((\rho\,e + p)\,u) = O(M\Delta x) + O\left((1 + \dfrac{\mathscr{E}_0}{M} + \dfrac{M}{\mathscr{E}_0})\Delta x\right) \\ \qquad\qquad + O\left((1-\mathscr{E}_0^2)(1+\theta)M\Delta x\right). \end{cases} \tag{78}$$

The proofs of the above propositions are written in Appendix G. In the low-Mach regime, the correction is by construction of order M. In areas where the solution is sufficiently smooth, it allows to reduce considerably the numerical diffusion induced by the momentum equation.

In the next section, one-dimensional numerical results of the present weighted splitting approach are presented.

6 Numerical Results

6.1 Ideal Gas Thermodynamics

In order to assess the above weighted splitting approach ability to follow slow contact discontinuities as well as fast shock fronts, a one-dimensional configurable shock-tube test-case is considered. The fluid has been firstly endowed with an ideal gas thermodynamics (13a) with the heat capacity ratio $\gamma = 7/5$. The simulation has been conducted on a domain of length $1\,m$, the initial discontinuity of the Riemann problem being located at $x = 0.5\,m$. The initial inputs of the Riemann problem are summed up on **Table 1**:

	Left state	Right state
$\rho\ (kg.m^{-3})$	$\rho_{0,\,L} = 1.$	$\rho_{0,\,R} = 0.125$
$u\ (m.s^{-1})$	$u_{0,\,L} = 0.$	$u_{0,\,R} = 0.$
$p\ (bar)$	$p_{0,\,L} = p_{0,\,R}\ (1 + \Delta)$	$p_{0,\,R} = 0.1$

Table 1: Ideal gas shock tube initial conditions

Recall that the analytical solution is made of a left rarefaction wave, a contact discontinuity propagating to the right and a right shock wave. The maximal Mach number is reached at the tail of the left rarefaction wave and can be controlled by increasing or diminishing Δ. When $\Delta = 9$, the classical Sod shock-tube described in [38] is retrieved, and the maximal Mach number M_{max} is about 0.92. We will refer to it as a Mach one case. When $\Delta = 2 \times 10^{-2}$, $M_{max} \approx 9.5 \times 10^{-2}$. This will be considered as an intermediate regime. Finally, when $\Delta = 8 \times 10^{-4}$, $M_{max} \approx 4.2 \times 10^{-3}$ and we call it low-Mach case.

In terms of quality measurement, three criteria have been studied: mesh convergence in L^1 norm, profiles of the different computed solutions and efficiency.

6.1.1 Convergence Curves

Convergence curves have been built using a wide range of cells number:

$N_{cells} \in \left\{10^2,\, 10^3,\, 10^4,\, 3 \times 10^4, 5 \times 10^4, 7 \times 10^4, 9 \times 10^4\right\}$. Convergence rates have been calculated with the last two points. For each variable of interest, three convergence curves are plotted according to the three different maximal Mach numbers defined above. Besides, five different schemes have been tested: "no-Sp" corresponds to the case where $\mathscr{E}_0^n = 1$ is imposed along the simulation. Thus, the weighted splitting is not triggered. "Sp-($\sqrt{M}$)" is

the weighted splitting approach with $\mathscr{E}_0^n = \max\left(\mathscr{E}_{inf}, \min\left(\sqrt{M_{max}^n}, 1\right)\right)$ while "Sp-(M)" involves the optimal $\mathscr{E}_0^n$ defined in formula (57). Eventually, "LP" is the Lagrange-Projection splitting method, fully described in [8] and taken as a benchmark. The mention "-corr" means that the low-Mach correction defined in (74) is triggered. Figure 4 corresponds to the velocity convergence curve while Figure 5 is associated to the pressure variable. Density convergence curve has intentionally not been plotted because results were extremely close.

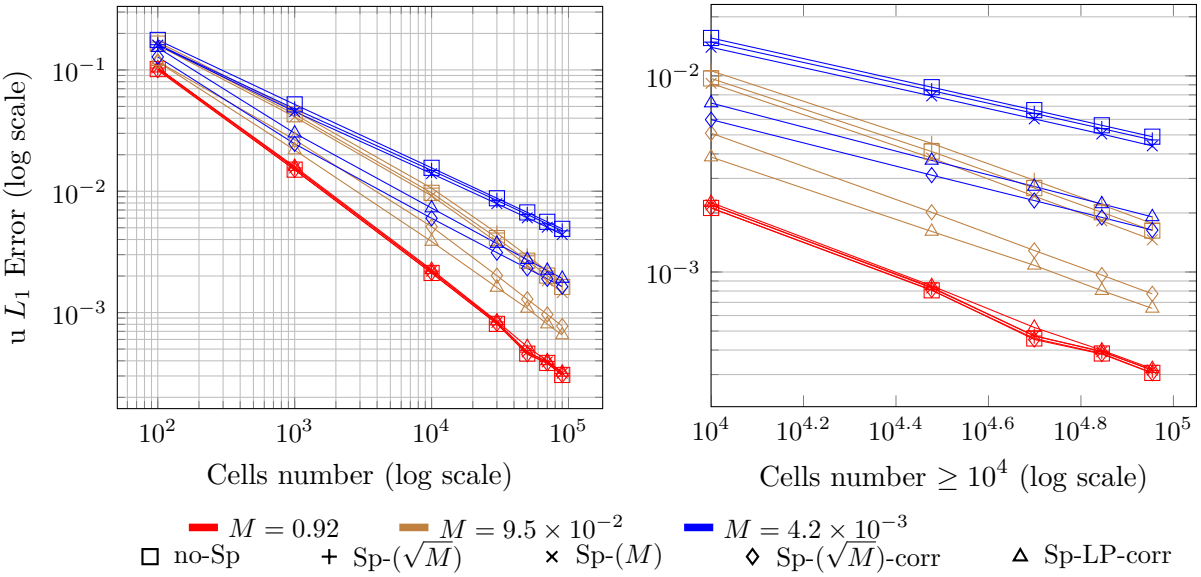

Figure 4: Velocity Convergence Curves

As it can be seen, every numerical scheme converges towards the analytical solution as mesh is refined. In the Mach one regime, convergence curves overlap quasi perfectly. It is coherent with the fact that, in such a regime, subsystem $\mathcal{C}$ is almost similar to the full Euler system. By construction, the numerical contribution of the acoustic subsystem $\mathcal{A}$ is negligible. Still, the proximity between the Lagrange-Projection scheme and the weighted splitting schemes is less straightforward.

Furthermore, as M_{max} decreases one can observe that the low-Mach corrected schemes Sp-($\sqrt{M}$)-corr and Sp-LP-corr are clearly more accurate than the other ones. For example on Figure 4, for $M = 9.5 \times 10^{-2}$, Sp-($\sqrt{M}$)-corr reaches the precision level of 2×10^{-3} with a 3×10^3 cells mesh whereas it requires more than 7×10^3 for No-Sp. This is in agreement with the acoustic truncation error result of **Proposition** 4 derived for a smooth solution. Moreover, as it can be seen on Figure 5, for $M = 4.2 \times 10^{-3}$, switching the weighting parameter $\mathscr{E}_0^n$ from $\sqrt{M_{max}^n}$ to its optimal value M_{max}^n has only a very slight positive effect on the scheme accuracy. This is due to the fact that, in case of low-Mach number flow, most of the numerical diffusion is generated by the acoustic part of the weighted splitting approach. To complete this comparison, one could have wished to see the case Sp-(M)-corr which, according to **Proposition** 5, is supposed to reduce the convective and acoustic numerical diffusion for a smooth solution initially in the well-prepared space. Unfortunately

this case suffers from strong non-physical oscillations located in the left rarefaction wave area. Plots of these oscillations for different cells numbers can be seen on Appendix F.

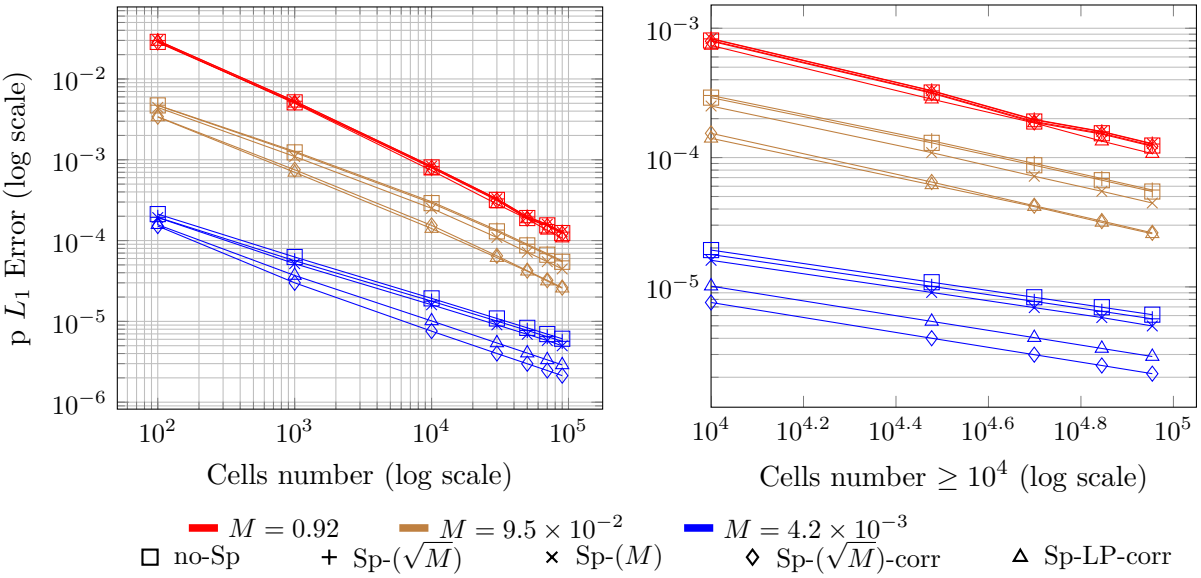

Figure 5: Pressure Convergence Curves

They have already been observed for low-Mach corrected numerical schemes written in Eulerian coordinates (see [22], chapter 3, section 3.G). However, these spurious perturbations are damped in the sense of the L^∞ and L^1 norms as mesh is refined. So far finding the optimal choice for the couple $(\mathscr{E}_0, \theta)$ in order to prevent the acoustic momentum flux from being completely centered and thus triggering such oscillations is still an open issue.

Let us do a last remark about the ability of these numerical schemes to approximate analytical solution when the Mach number tends to zero. This can be measured by studying the convergence rates of the different curves as Mach tends towards zero.

	$M = 0.92$	$M = 9.5 \times 10^{-2}$	$M = 4.2 \times 10^{-3}$
No-Sp	0.870	0.803	0.530
Sp-($\sqrt{M}$)	0.868	0.814	0.531
Sp-M	0.860	0.829	0.597
Sp-($\sqrt{M}$)-corr	0.868	0.833	0.580
Sp-LP-corr	0.882	0.806	0.572
HLLC	0.879	0.802	0.528

Table 2: Pressure Convergence Rate (L^1 norm)

Table 2 presents these orders of convergence for pressure. One can see that for *every* schemes based on a splitting, the order of convergence is depreciated as the Mach number decreases. Indeed for pressure, it passes from 0.87 at $M = 0.92$ (the expected order already obtained in [20]) to 0.82 at $M = 9.5 \times 10^{-2}$ and 0.56 in the low-Mach case. Seeking to

confirm this behavior, the same test case has been computed using an HLLC-type scheme [42]; once again, at $M = 4.2 \times 10^{-3}$ the convergence rate is 0.528. This suggests that: the lowest the Mach number is, the slowest Godunov-like schemes are to reach the analytical solution as mesh is refined. The same order of magnitude seems to be found in [19] for a double rarefaction wave problem performed on Euler barotropic system with $M \approx 3.1 \times 10^{-2}$. The implicit-explicit AP scheme used to obtain this order is based on a Rusanov spatial discretization. One could think that this result stresses a behavior already noticed in [25] and [24] for steady cases: Godunov-like schemes have difficulty to converge towards the low-Mach (incompressible) solution. Further investigations have to be undertaken in order to understand this trend.

Beyond convergence curves and rates, one must also have a look on the solution profile obtained with the different numerical schemes at a fixed mesh size. This is done in the next subsection.

6.1.2 Solution Profiles

Figure 6 and Figure 7 show the velocity and pressure final profiles calculated with the different numerical solutions in the low-Mach regime. We only plot the left rarefaction and the right shock waves through which u and p change. Mesh is made of $N_{cells} = 10^3$ cells.

One can notice that No-Sp is always the most diffusive scheme. Besides, the positive effect of the $\mathscr{E}_0^n = \max\left(\mathscr{E}_{inf}, \min\left(M_{max}^n, 1\right)\right)$ choice compared to $\mathscr{E}_0^n = \max\left(\mathscr{E}_{inf}, \min\left(\sqrt{M_{max}^n}, 1\right)\right)$ is exclusively located in the left rarefaction wave fan where the solution is continuous. In addition, No-Sp, Sp-$(\sqrt{M})$ and Sp-(M) profiles overlap in the shock front region.

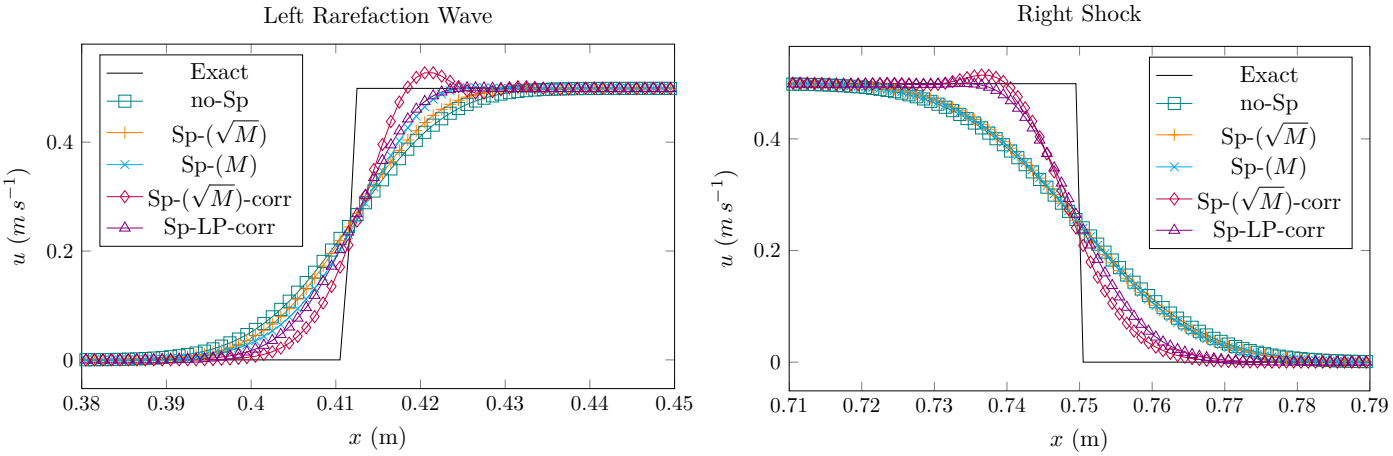

Figure 6: Velocity profile at $M = 4.2 \times 10^{-3}$, with $N_{cells} = 10^3$

Eventually, the low-Mach correction globally improves the computed solution accuracy. The Sp-$(\sqrt{M})$-corr case produces profiles closer to the analytical solution than Sp-LP-corr at the cost of little overshoots in the tail of the left rarefaction wave and before the shock front.

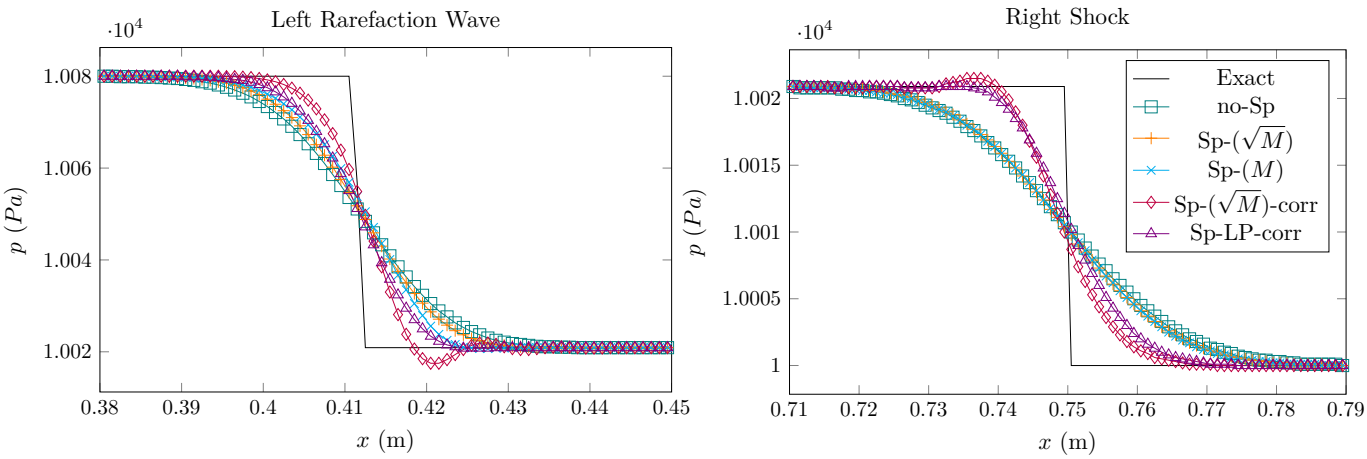

Figure 7: Pressure profile at $M = 4.2 \times 10^{-3}$, with $N_{cells} = 10^3$

6.1.3 Efficiency Curve

Computational cost at fixed accuracy level is now investigated. Figure 8 and Figure 9 describe the pressure efficiency curves of the different numerical schemes for the three Mach regimes. In the Mach one regime, every schemes seem to behave equivalently, the proposed weighted splitting approach requiring slightly more CPU time than No-Sp or Sp-LP-corr. When $M = 9.5 \times 10^{-2}$, the weighted splitting approach is still slower than No-Sp, however the low-Mach corrected schemes are clearly less time consuming, at fixed error than the other ones. Indeed Sp-($\sqrt{M}$)-corr and Sp-LP-corr reach the precision of 7×10^{-5} in about one hour and a half whereas it requires six hours for No-Sp and more than seven hours for Sp-($\sqrt{M}$). Eventually, in the low-Mach case, Sp-($\sqrt{M}$)-corr seems to produce better results than Sp-LP-corr. For a fixed precision of 4×10^{-6} the weighted splitting method needs about one hour and forty minutes whereas the Lagrange-Projection method requires a little less than three hours.

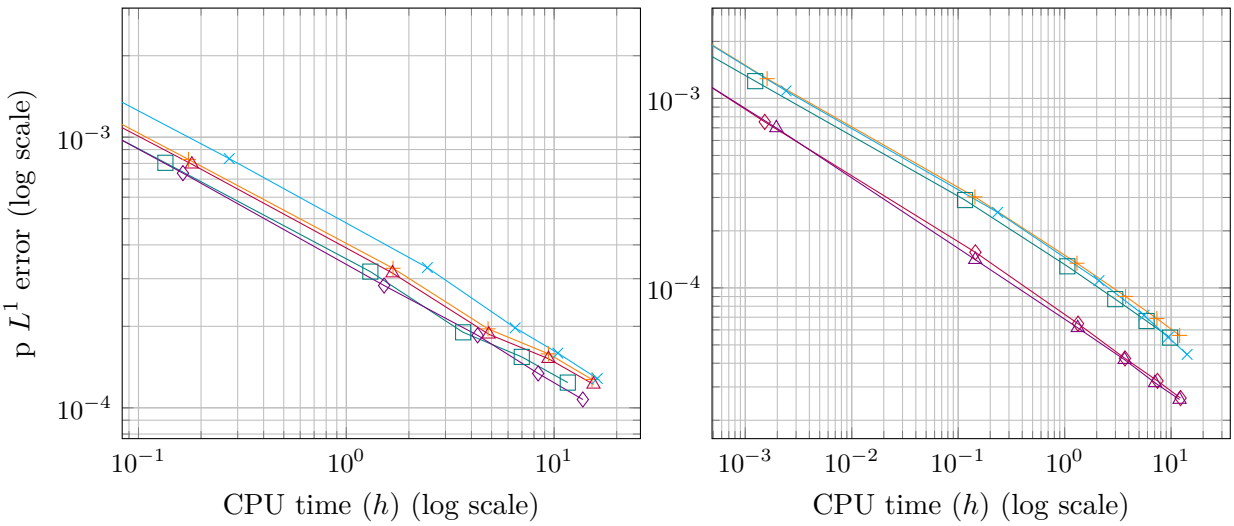

Figure 8: Pressure Efficiency Curves: $M = 0.92$ (left), $M = 9.5 \times 10^{-2}$ (right)

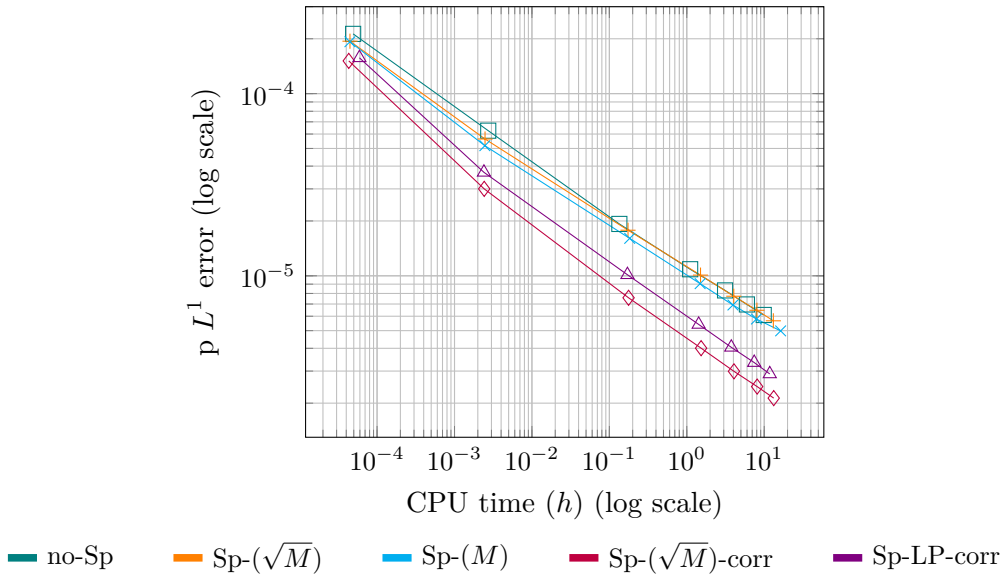

Figure 9: Pressure Efficiency Curves: $M = 4.2 \times 10^{-3}$

6.2 Stiffened Gas Thermodynamics

In the above subsection, some elements seem to suggest that the weighted splitting approach produces satisfying results for a wide range of Mach number when the fluid is modeled as an ideal gas. A natural extension is the stiffened gas thermodynamics (14a) which strengthen the quasi-incompressible property of the studied fluid. Then, new initial conditions for the Riemann problem have been defined on Table 3. As it can be seen, initial density is of

order $10^3\,kg\,m^{-3}$ while pressure jump is 3 bars. The heat capacity ratio of the stiffened gas law is $\gamma = 7.5$ whereas $P_\infty = 3 \times 10^8\,Pa$. These two constants have been taken in order to produce sound speeds $c = \sqrt{\gamma(p + P_\infty)/\rho} \approx \sqrt{\gamma\, P_\infty/\rho}$ of order $1500\,m\,s^{-1}$ like in water at atmospheric conditions and a temperature of 295 K. In this case the maximal Mach number is about $M_{max} \approx 4.6 \times 10^{-5}$. Thus, we are still in a very low-Mach regime.

	Left state	Right state
$\rho\ (kg.m^{-3})$	$\rho_{0,\,L} = 10^3$	$\rho_{0,\,R} = 9 \times 10^2$
$u\ (m.s^{-1})$	$u_{0,\,L} = 0.$	$u_{0,\,R} = 0.$
$p\ (bar)$	$p_{0,\,L} = 3$	$p_{0,\,R} = 1$

Table 3: Stiffened gas shock tube initial conditions

6.2.1 Acoustic Relaxation Coefficient Calibration

Let us go back to **Remark 5**. Testing a stiffened gas thermodynamics allows to compare the acoustic subcharacteristic condition (37b) derived from the weighted splitting approach and (39) obtained directly from the relaxation of the full Euler system and found in [22]. Let us recall that the inferior bound of (37b) uses an artificial acoustic sound speed $c_{\mathcal{A}}$ whereas (39) is based on the physical sound speed c. In the previous ideal gas thermodynamics case $c_{\mathcal{A}} = \sqrt{(\gamma-1)p/\rho} = \sqrt{(\gamma-1)/\gamma}\,c$ and $\sqrt{(\gamma-1)/\gamma} \approx 0.53$ such that this non-physical acoustic celerity was of the same order that the real sound speed. However, with a stiffened gas thermodynamics, $c_{\mathcal{A}}$ does not change while c becomes $\sqrt{\gamma\,(p+P_\infty)/\rho} \approx \sqrt{\gamma\, P_\infty/\rho}$. Thus $c_{\mathcal{A}}/c \approx \sqrt{(\gamma-1)/\gamma}\,\sqrt{p/P_\infty} \ll 1$. One could wonder if considering the subcharacteristic condition (37b) based on a non-physical celerity rather than the one based on the real sound speed (39) has an effect on the overall scheme accuracy? So far, numerical arguments seem to go in favor of an acoustic relaxation coefficient based on the real sound speed. Indeed, Figure 10 shows two weighted splitting simulations of type Sp-($\sqrt{M}$). The first one, noted Sp-($\sqrt{M}$)-$a_{\mathcal{A}}$, takes the subcharacteristic condition (37b) into account whereas the second one, Sp-($\sqrt{M}$)-a_E, involves (39). The mesh was composed of 10^3 cells.

It turns out that Sp-($\sqrt{M}$)-$a_{\mathcal{A}}$ produces non-physical oscillations inside the rarefaction fan and before the shock front. Things are even worse when Sp-(M)-$a_{\mathcal{A}}$ and Sp-(M)-a_E are compared. Indeed, even if the non-physical subcharacteristic condition (37b) is fulfilled, the amplitude of the spurious oscillations is such that pressure becomes negative after several timesteps. Simulation crashes because $c_{\mathcal{A}}$ becomes a complex number. On the contrary, Sp-(M)-a_E does not suffer from any oscillations or stability issues. Recall that the relaxation coefficient $a_{\mathcal{A}}$ multiplies the non-centered part of the acoustic momentum flux responsible for most of the numerical diffusion of the scheme. Hence, by considering subcharacteristic condition (39) rather than (37b) this coefficient has been considerably increased as well as the numerical diffusion coefficient. Non-physical oscillations are then removed. Nevertheless, a theoretical motivation for preferring (39) instead of (37b) it is still to be found.

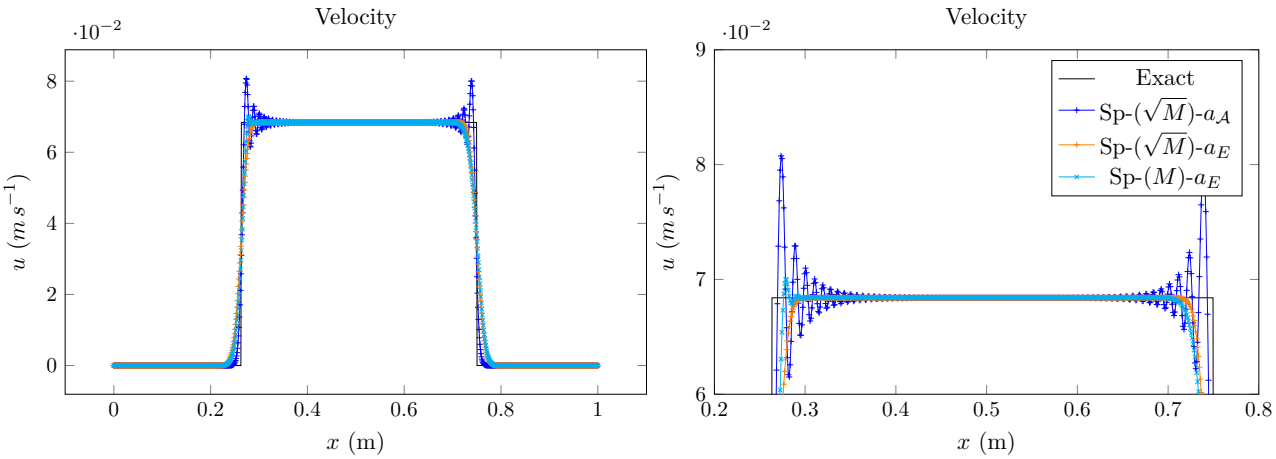

Figure 10: Effect of the Estimation of the Relaxation Coefficient

In the sequel, the acoustic relaxation coefficient $a_{\mathcal{A}}$ has been calculated using the physical sound speed: $a_{\mathcal{A}} > \rho\, c$. The global CFL condition (60) is modified in consequence.

6.2.2 Convergence Curves and Computed Solutions Profiles

Similarly to the ideal gas thermodynamics configuration, pressure convergence curve plotted on Figure 11 shows that the low-Mach corrected schemes are the most accurate as mesh is refined. However, one can notice that the Sp-($\sqrt{M}$)-corr curve remains above of the LP one until $N_{cells} \geq 5 \times 10^4$. This can be explained by observing the solutions profiles drawn on Figure 12. The low-Mach correction centers the pressure flux since the Mach number is very small in every computational region. Hence, it triggers oscillations in areas where the solution is sharp. Such oscillations are present in the case of Sp-LP-corr but their amplitude is smaller. So far this difference remains unexplained. In any case, the more the mesh is refined, the more localized are these oscillations. For $N_{cells} = 9 \times 10^4$ the Sp-($\sqrt{M}$)-corr becomes more accurate than the Sp-LP-corr one. This sudden descent can be measured by pressure convergence rate written on **Table 4** which is 0.783 for Sp-($\sqrt{M}$)-corr contrary to Sp-LP-corr which only reaches 0.561. Additional points should be added to see the trend evolution.

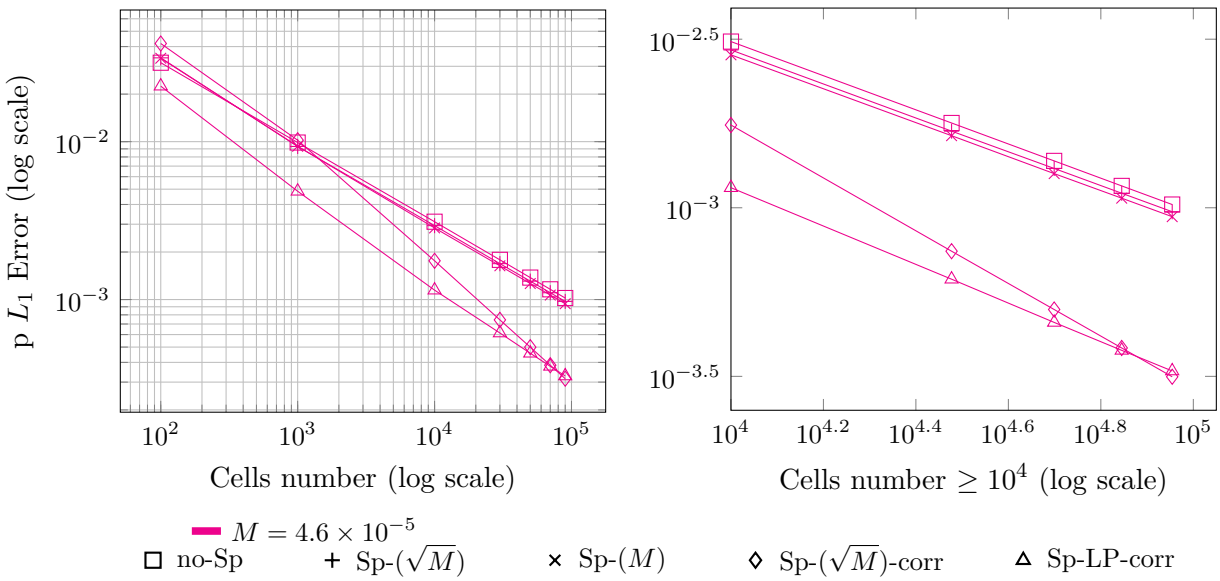

Figure 11: Pressure Convergence Curve

	$M = 4.6 \times 10^{-5}$
No-Sp	0.506
Sp-($\sqrt{M}$)	0.502
Sp-M	0.503
Sp-($\sqrt{M}$)-corr	0.783
Sp-LP-corr	0.561

Table 4: Pressure Convergence Rate (L^1 norm)

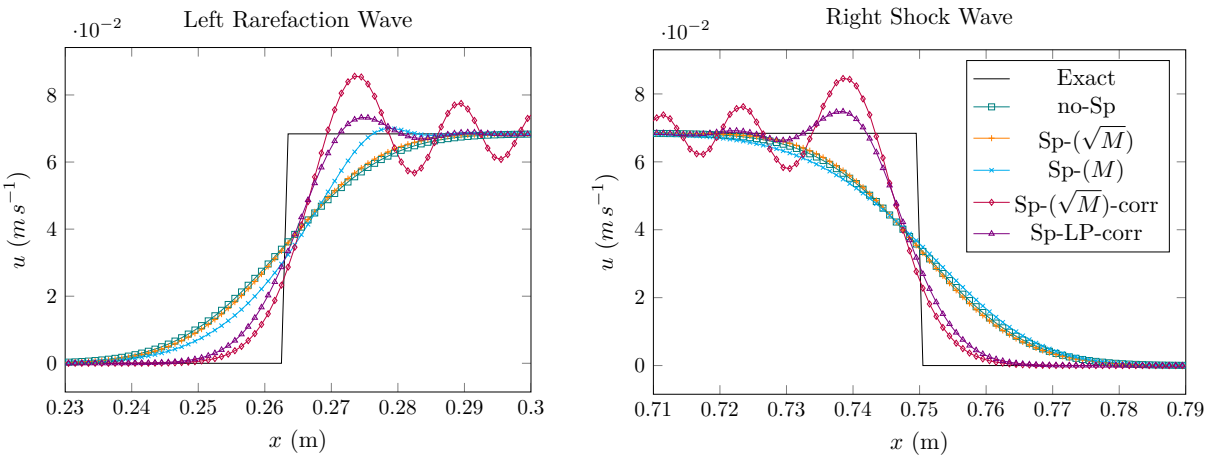

Figure 12: Velocity Profile at $M = 4.6 \times 10^{-5}$ with $N_{cells} = 10^3$

7 Conclusion

In this work, a conservative fractional step approach based on a time-weighted splitting has been proposed for Euler-like models. The weighting parameter is proportional to the instantaneous maximal flow Mach number M. When the latter takes high values the splitting allows to directly solve the overall Euler-like system in one step with an explicit time integration. Thus, shock waves are correctly captured without any diffusion or dispersion induced by the acoustic implicitation process. On the contrary, if M is close to zero, convection is completely decoupled from acoustic. In that case, the acoustic discrete flux is modified by a stable low-Mach correction. This results in a uniform truncation error with respect to M for smooth and initially well-prepared solutions.

What is more, the Suliciu-like relaxation method used to discretize both convective and acoustic subsystems provides the density and internal energy positivity under the introduction of new admissible lower bounds for the relaxation constants. Besides, such relaxation constants encapsulate the thermodynamic nonlinearity and offer an easy way to deal with general equations of state.

The one-dimensional results performed with an ideal and a stiffened gas thermodynamics show that the weighted splitting approach is as accurate and efficient as the Lagrange-Projection method [8] for a wide range of Mach numbers.

Additional developments whose results are presented in [28, 29] deal with the adaptation of the acoustic implicitation technique proposed in [13, 8] to the present splitting. Particularly, if one is interested in following the material waves of low-Mach number flows, the implicit-explicit version of the present approach avoids the time-diffusion issues described in the introduction. However, when applied to the non-stationary low-Mach number shock tubes described above, the implicit-explicit strategy seems to be less efficient than a full time-explicit resolution; meaning that at a given error level, it is still more CPU-consuming. This echoes a difficulty pointed out in the introduction: a slightly compressible fluid flow can

generate high-amplitude pressure waves even if the flow Mach number is small; and acoustic implicitation methods based on a material Courant number seem to damp them. Another improvement would concern the definition of the discrete weighting parameter $\mathscr{E}_0^n$: in the same manner as for the relaxation constants, it could be transformed in a local weighting factor $(\mathscr{E}_0)_{i+1/2}^n = \max\left(\mathscr{E}_{inf}, \min\left(\max(M_i^n, M_{i+1}^n), 1\right)\right)$ which is spatially constant for the Riemann problem solved at the interface. By doing so, the present weighted splitting approach could react to the spatial fluctuations of the flow Mach number and could improve even further the global accuracy of the method. Eventually, a reflection about the relevance of an extension of the present weighted splitting approach to homogeneous relaxed models will be undertaken.

Acknowledgements

The first author received a financial support through the EDF-CIFRE contract 0561-2015. Computational facilities were provided by EDF.

Appendix A

For the sake of simplicity, we prove **Proposition** 1 in 1D. Let us consider the set of non conservative variables $\mathbf{V} = [\rho,\, u,\, p]^T$. If the solutions of subsystems $\mathcal{C}$ and $\mathcal{A}$ are smooth, one can rewrite them equivalently as:

$$\mathcal{C}^{NC}: \begin{cases} \partial_t \rho + u\,\partial_x \rho + \rho\,\partial_x u = 0 \\ \partial_t u + u\,\partial_x u + \dfrac{1}{\rho}\partial_x\left(\mathscr{E}_0^2(t)\,p\right) = 0 \\ \partial_t p + u\,\partial_x p + \rho\, c_{\mathcal{C}}^2\,\partial_x u = 0 \end{cases} \qquad \mathcal{A}^{NC}: \begin{cases} \partial_t \rho = 0 \\ \partial_t u + \dfrac{1}{\rho}\partial_x\left((1-\mathscr{E}_0^2(t))\,p\right) = \underline{0} \\ \partial_t p + (1-\mathscr{E}_0^2(t))\rho\, c_{\mathcal{A}}^2\partial_x u = 0 \end{cases} \tag{79}$$

(80)

In variables $\mathbf{V}$ the Jacobian matrices of subsystems $\mathcal{C}^{NC}$ and $\mathcal{A}^{NC}$ are:

$$\mathcal{C}^{NC}: \begin{bmatrix} u & \rho & 0 \\ 0 & u & \mathscr{E}_0^2/\rho \\ 0 & \rho\, c_{\mathcal{C}}^2 & u \end{bmatrix} \tag{81} \qquad \mathcal{A}^{NC}: \begin{bmatrix} 0 & 0 & 0 \\ 0 & 0 & (1-\mathscr{E}_0^2)/\rho \\ 0 & (1-\mathscr{E}_0^2)\rho\, c_{\mathcal{A}}^2 & 0 \end{bmatrix} \tag{82}$$

Supposing that $c_{\mathcal{C}}^2 \geq 0$ and $c_{\mathcal{A}}^2 \geq 0$, the eigenvalues and eigenvectors can be easily obtained and read:

$$\mathcal{C}^{NC}: \begin{array}{l} \lambda_1^{\mathcal{C}} = u - \mathscr{E}_0\, c_{\mathcal{C}} \\ \lambda_2^{\mathcal{C}} = u \\ \lambda_3^{\mathcal{C}} = u + \mathscr{E}_0\, c_{\mathcal{C}} \end{array} \qquad \mathbf{r}_1^{\mathcal{C}} = \begin{bmatrix} \rho \\ -\mathscr{E}_0\, c_{\mathcal{C}} \\ \rho\, c_{\mathcal{C}}^2 \end{bmatrix},\ \mathbf{r}_2^{\mathcal{C}} = \begin{bmatrix} 1 \\ 0 \\ 0 \end{bmatrix},\ \mathbf{r}_3^{\mathcal{C}} = \begin{bmatrix} \rho \\ +\mathscr{E}_0\, c_{\mathcal{C}} \\ \rho\, c_{\mathcal{C}}^2 \end{bmatrix}, \tag{83}$$

$$\mathcal{A}^{NC}: \begin{array}{ll} \lambda_1^{\mathcal{A}} = -\left(1-\mathscr{E}_0^2\right) c_{\mathcal{A}} & \\ \lambda_2^{\mathcal{A}} = 0 & \mathbf{r}_1^{\mathcal{A}} = \begin{bmatrix} 0 \\ 1 \\ -\rho\, c_{\mathcal{A}} \end{bmatrix},\ \mathbf{r}_2^{\mathcal{A}} = \begin{bmatrix} 1 \\ 0 \\ 0 \end{bmatrix},\ \mathbf{r}_3^{\mathcal{A}} = \begin{bmatrix} 0 \\ 1 \\ \rho\, c_{\mathcal{A}} \end{bmatrix}, \\ \lambda_3^{\mathcal{A}} = \left(1-\mathscr{E}_0^2\right) c_{\mathcal{A}} & \end{array} \tag{84}$$

Then one can notice that, for the two subsystems, the 1-field and 3-field are genuinely non linear whereas the 2-field is linearly degenerate. Let us now study the sufficient conditions for which $c_{\mathcal{C}}^2 \geq 0$ and $c_{\mathcal{A}}^2 \geq 0$. Consider the ideal gas thermodynamics presented in equation (13). Then:

$$\begin{aligned} c_{\mathcal{C}}^2 &= \left(1+\mathscr{E}_0^2(\gamma-1)\right)\frac{p}{\rho} = \gamma_{\mathscr{E}_0}\,\frac{p}{\rho} \\ c_{\mathcal{A}}^2 &= (\gamma-1)\frac{p}{\rho} \end{aligned} \tag{85}$$

Since $\mathscr{E}_0^2 \in [0,\,1]$, $\gamma_{\mathscr{E}_0} \in [1,\,\gamma]$. What is more the ideal gas phase-space ensures that p is positive too. Thus, in case of an ideal gas thermodynamics, $c_{\mathcal{C}}^2$ and $c_{\mathcal{A}}^2$ are naturally positive. On the contrary, when the stiffened gas thermodynamics is at stake one obtains:

$$\begin{aligned} c_{\mathcal{C}}^2 &= \frac{\gamma_{\mathscr{E}_0}\,p + \gamma P_\infty}{\rho} \\ c_{\mathcal{A}}^2 &= (\gamma-1)\frac{p}{\rho} \end{aligned} \tag{86}$$

The stiffened gas phase-space ensures that $p > -P_\infty \Rightarrow \gamma_{\mathscr{E}_0}\,p + \gamma\,P_\infty > (\gamma - \gamma_{\mathscr{E}_0})\,P_\infty$. And $\gamma - \gamma_{\mathscr{E}_0}$ is positive. Once again, $c_{\mathcal{C}}^2$ is positive without any condition. However $c_{\mathcal{A}}^2 \geq 0 \Leftrightarrow p \geq 0$ which is not guaranteed in the stiffened gas case.

Appendix B

Consider Ω a bounded spatial domain of $\mathbb{R}^d$, $d \in \{1,\,2,\,3\}$ which boundary is $\partial\,\Omega$. The specific internal energy of both subsystems verifies the following PDEs:

$$\begin{cases} \partial_t\,\varepsilon + \mathbf{u}\cdot\underline{\nabla}\,\varepsilon + \mathscr{E}_0^2(t)\,\dfrac{p}{\rho}\,\underline{\nabla}\cdot(\mathbf{u}) = 0 \quad (\mathcal{C}) \\ \partial_t\,\varepsilon + \left(1-\mathscr{E}_0^2(t)\right)\,\dfrac{p}{\rho}\,\underline{\nabla}\cdot(\mathbf{u}) = 0 \qquad (\mathcal{A}) \end{cases} \tag{87}$$

Consider $\varepsilon^- = \dfrac{\varepsilon - |\varepsilon|}{2}$ the negative part of the specific internal energy. Consider the following hypothesis about the solution's smoothness and the initial and boundary

conditions:

$$\forall t \geq 0,\ \mathbf{u}(t,.) \in L^{\infty}(\Omega),\ \underline{\nabla} \cdot (\mathbf{u})(t,.) \in L^{\infty}(\Omega) \tag{88a}$$
$$\forall t \geq 0,\ \varepsilon(t,.) \in L^{\infty}(\Omega),\ \underline{\nabla}(\varepsilon)(t,.) \in L^{\infty}(\Omega)^{d} \tag{88b}$$
$$\forall t \geq 0,\ \frac{p}{\rho}(t,.) \in L^{\infty}(\Omega) \tag{88c}$$
$$\forall \mathbf{x} \in \Omega,\ \varepsilon(0,\mathbf{x}) > 0 \Leftrightarrow \varepsilon^{-}(0,\mathbf{x}) = 0 \tag{88d}$$
$$\varepsilon_{|\partial\Omega} \geq 0 \text{ if } \mathbf{u} \cdot \mathbf{n}_{|\partial\Omega} \leq 0 \tag{88e}$$

By multiplying equation (87) by ε^{-} and integrating over Ω one obtains:

$$\begin{cases} \dfrac{d}{dt}\displaystyle\int_{\Omega} \frac{(\varepsilon^{-})^2}{2}\, d\Omega + \int_{\Omega} \mathbf{u} \cdot \underline{\nabla} \frac{(\varepsilon^{-})^2}{2}\, d\Omega + \int_{\Omega} \mathscr{E}_0^2(t)\, \frac{\varepsilon^{-} p}{\rho}\, \underline{\nabla} \cdot (\mathbf{u})\, d\Omega = 0 & (\mathcal{C}) \\ \dfrac{d}{dt}\displaystyle\int_{\Omega} \frac{(\varepsilon^{-})^2}{2}\, d\Omega + \int_{\Omega} \left(1 - \mathscr{E}_0^2(t)\right)\, \frac{\varepsilon^{-} p}{\rho}\, \underline{\nabla} \cdot (\mathbf{u})\, d\Omega = 0 & (\mathcal{A}) \end{cases} \tag{89}$$

By using Green's formula the above equations can be transformed into:

$$\begin{cases} \dfrac{d}{dt}\dfrac{||\varepsilon^{-}||_{L^2}^2}{2} = \displaystyle\int_{\Omega} \underline{\nabla} \cdot (\mathbf{u}) \left(\frac{(\varepsilon^{-})^2}{2} - \mathscr{E}_0^2(t)\, \frac{\varepsilon^{-} p}{\rho} \right) d\Omega - \int_{\partial\Omega} \frac{(\varepsilon^{-})^2}{2} \mathbf{u} \cdot \mathbf{n}\, d\Gamma & (\mathcal{C}) \\ \dfrac{d}{dt}\dfrac{||\varepsilon^{-}||_{L^2}^2}{2} = -\displaystyle\int_{\Omega} \underline{\nabla} \cdot (\mathbf{u}) \left(1 - \mathscr{E}_0^2(t)\right)\, \frac{\varepsilon^{-} p}{\rho}\, d\Omega & (\mathcal{A}) \end{cases} \tag{90}$$

If the ideal gas thermodynamics is considered, $\dfrac{\varepsilon^{-} p}{\rho} = (\gamma - 1)(\varepsilon^{-})^2$. Because of the admissible inlet boundary condition (88e), $-\displaystyle\int_{\partial\Omega} \frac{(\varepsilon^{-})^2}{2} \mathbf{u} \cdot \mathbf{n}\, d\Gamma$ is always negative so that we can derive the following inequalities:

$$\begin{cases} \dfrac{d}{dt}\dfrac{||\varepsilon^{-}||_{L^2}^2}{2} \leq \overbrace{\underset{\Omega}{sup} \left| \underline{\nabla} \cdot (\mathbf{u}) \left(1 - 2\, \mathscr{E}_0^2(t)\, (\gamma - 1)\right) \right|}^{L_{\mathcal{C}}(t)} \dfrac{||\varepsilon^{-}||_{L^2}^2}{2} & (\mathcal{C}) \\ \dfrac{d}{dt}\dfrac{||\varepsilon^{-}||_{L^2}^2}{2} \leq \underbrace{\underset{\Omega}{sup} \left| 2\, \underline{\nabla} \cdot (\mathbf{u}) \left(1 - \mathscr{E}_0^2(t)\right) (\gamma - 1) \right|}_{L_{\mathcal{A}}(t)} \dfrac{||\varepsilon^{-}||_{L^2}^2}{2} & (\mathcal{A}) \end{cases} \tag{91}$$

Thus, because of Gronwall's lemma:

$$\begin{cases} ||\varepsilon^{-}||_{L^2}^2(t) <\leq ||\varepsilon^{-}||_{L^2}^2(0)\, e^{\int_0^t L_{\mathcal{C}}(s)\, ds} = 0 \Rightarrow ||\varepsilon^{-}||_{L^2}^2(t) = 0 & (\mathcal{C}) \\ ||\varepsilon^{-}||_{L^2}^2(t) \leq ||\varepsilon^{-}||_{L^2}^2(0)\, e^{\int_0^t L_{\mathcal{A}}(s)\, ds} = 0 \Rightarrow ||\varepsilon^{-}||_{L^2}^2(t) = 0 & (\mathcal{A}) \end{cases} \tag{92}$$

One can notice that, beyond hypothesis presented in (88), a sufficient condition to derive inequalities (91) is $\dfrac{p}{\rho} = O\left(\varepsilon^{-}\right)$ on Ω.

When a stiffened gas thermodynamics defined by (14a) and (14b) is at stake, one is interested in the positivity of $P = \rho\,\varepsilon - P_\infty$. Such a variable follows the PDEs:

$$\begin{cases} \partial_t P + \underline{\nabla}\cdot(P\,\mathbf{u}) + \mathscr{E}_0^2(t)\,(\gamma-1)\,P\,\underline{\nabla}\cdot(\mathbf{u}) + P_\infty\,(1-\mathscr{E}_0^2(t))\,\underline{\nabla}\cdot\mathbf{u} = 0, & (\mathcal{C}) \\ \partial_t P + (1-\mathscr{E}_0^2(t))\,(\gamma-1)\,P\,\underline{\nabla}\cdot(\mathbf{u}) - P_\infty\,(1-\mathscr{E}_0^2(t))\,\underline{\nabla}\cdot\mathbf{u} = 0. & (\mathcal{A}) \end{cases} \tag{93}$$

By doing exactly the same kind of hypothesis and calculations than for the ideal case, one can obtain:

$$\begin{cases} \dfrac{d}{dt}\,||P^-||_{L^2}^2 \leq (2\,\mathscr{E}_0^2\,(\gamma-1)+1)\,\underset{\Omega}{sup}\,|\underline{\nabla}\cdot\mathbf{u}|\,||P^-||_{L^2}^2 - (1-\mathscr{E}_0^2(t))\,P_\infty\displaystyle\int_\Omega P^-\underline{\nabla}\cdot(\mathbf{u})\,d\Omega, & (\mathcal{C}) \\ \dfrac{d}{dt}\,||P^-||_{L^2}^2 \leq 2\,(1-\mathscr{E}_0^2)(\gamma-1)\,\underset{\Omega}{sup}\,|\underline{\nabla}\cdot\mathbf{u}|\,||P^-||_{L^2}^2 + (1-\mathscr{E}_0^2(t))\,P_\infty\displaystyle\int_\Omega P^-\underline{\nabla}\cdot(\mathbf{u})\,d\Omega. & (\mathcal{A}) \end{cases} \tag{94}$$

Because $1/P^-$ is a priori not bounded, it is not possible to bound the last term in equations (94) by a positive quantity times $||P^-||_{L^2}^2$ except in the $\mathscr{E}_0^2(t)=1$ or $P_\infty = 0$ cases. Thus, Gronwall's lemma cannot be applied and one cannot be sure that $||P^-||_{L^2}(t) = 0$.

Appendix C

Consider the Riemann problem presented on Figure 1 related to the convective subsystem. It produces intermediate states described in relations (46) and (47). Let us find a sufficient condition on the subcaracteristic coefficient $a_\mathcal{C}$ so that the intermediate densities $\rho_{k,\mathcal{C}}^*,\ k \in \{L,\ R\}$ are positive.

$$\begin{aligned} \rho_{k,\mathcal{C}}^* \geq 0 &\Leftrightarrow \tau_{k,\mathcal{C}}^* \geq 0 \\ &\Leftrightarrow \tau_k + \frac{(-1)^{i_k+1}}{\mathscr{E}_0\,a_\mathcal{C}}\,(u_\mathcal{C}^* - u_k) \geq 0 \\ &\Leftrightarrow a_\mathcal{C}^2 + \frac{\rho_k\,(u_R-u_L)}{2\mathscr{E}_0}\,a_\mathcal{C} + \frac{(-1)^{i_k}\rho_k\,(p_R-p_L)}{2} \geq 0 \end{aligned} \tag{95}$$

The second order polynomial function admits real roots if and only if $\Delta_k^\rho \equiv \dfrac{\rho_k\,(u_R-u_L)^2}{8\,\mathscr{E}_0^2} + (-1)^{i_k+1}\,(p_R-p_L) \geq 0$. Let us notice that $\Delta_L^\rho < 0 \Rightarrow \Delta_R^\rho > 0$ and conversely. In that case the polynomial constraint (95) related to Δ_L^ρ is automatically verified. Thus, consider the most demanding case where $\Delta_L^\rho \geq 0$ and $\Delta_R^\rho \geq 0$, namely:

$$-\frac{\rho_L\,(u_R-u_L)^2}{8} \leq \mathscr{E}_0^2\,(p_R-p_L) \leq \frac{\rho_R\,(u_R-u_L)^2}{8} \tag{96}$$

If $u_L \neq u_R$, inequality (96) holds easily with low-Mach flows when $\mathscr{E}_0$ tends toward zero.

Let us define $a_k^\rho,\ k \in \{L,\ R\}$ the highest roots related to the above polynomial functions:

$$
\begin{aligned}
a_L^\rho &\equiv \frac{1}{2}\left(-\frac{\rho_L\,(u_R-u_L)}{2\,\mathscr{E}_0}+\sqrt{\frac{\rho_L^2\,(u_R-u_L)^2}{4\,\mathscr{E}_0^2}+2\,\rho_L\,(p_R-p_L)}\right)\\
a_R^\rho &\equiv \frac{1}{2}\left(-\frac{\rho_R\,(u_R-u_L)}{2\,\mathscr{E}_0}+\sqrt{\frac{\rho_R^2\,(u_R-u_L)^2}{4\,\mathscr{E}_0^2}-2\,\rho_R\,(p_R-p_L)}\right)
\end{aligned}
\tag{97}
$$

By noticing that $\forall A \geq 0, -A+\sqrt{A^2+B} > 0 \Leftrightarrow B > 0$, one can build the following table which gives the sign of a_L^ρ and a_R^ρ:

	$u_R > u_L$	$u_R < u_L$
$p_R > p_L$	$a_L^\rho > 0$, $a_R^\rho < 0$	$a_L^\rho > 0$, $a_R^\rho > 0$
$p_R < p_L$	$a_L^\rho < 0$, $a_R^\rho > 0$	$a_L^\rho > 0$, $a_R^\rho > 0$

Table 5: Positivity Domain of a_L^ρ and a_R^ρ

In practice, when either a_L^ρ or a_R^ρ are positive, we add it as an additional constraint into the subcaracteristic condition (37a) leading to the modified subcaracteristic condition (63).

The non-dimensional expressions of a_L^ρ and a_R^ρ are:

$$
\begin{aligned}
a_L^\rho &\equiv \frac{1}{2}\left(-\frac{M}{\mathscr{E}_0}\frac{\rho_L\,(u_R-u_L)}{2}+\sqrt{\left(\frac{M}{\mathscr{E}_0}\right)^2\frac{\rho_L^2\,(u_R-u_L)^2}{4}+2\,\rho_L\,(p_R-p_L)}\right)\\
a_R^\rho &\equiv \frac{1}{2}\left(-\frac{M}{\mathscr{E}_0}\frac{\rho_R\,(u_R-u_L)}{2}+\sqrt{\left(\frac{M}{\mathscr{E}_0}\right)^2\frac{\rho_R^2\,(u_R-u_L)^2}{4}-2\,\rho_R\,(p_R-p_L)}\right)
\end{aligned}
\tag{98}
$$

Thus, if $\mathscr{E}_0$ is proportional to the Mach number as defined in (70), the above non-dimensional roots are of order one.

Concerning the equivalence between the intermediate density positivity and the ordering of the eigenvalues of subsystem $\mathcal{C}^\mu$, one can notice that:

$$
\begin{aligned}
&u_L - \mathscr{E}_0\,a_{\mathcal{C}}\,\tau_L \leq u_{\mathcal{C}}^*\\
&\Leftrightarrow 0 \leq \mathscr{E}_0\,a_{\mathcal{C}}\left(\tau_L+\frac{1}{\mathscr{E}_0\,a_{\mathcal{C}}}\,(u_{\mathcal{C}}^*-u_L)\right)\\
&\Leftrightarrow 0 \leq \tau_{L,\mathcal{C}}^*
\end{aligned}
\tag{99}
$$

By doing the same calculation, one can see that $u_{\mathcal{C}}^* \leq u_R + \mathscr{E}_0\,a_{\mathcal{C}}\,\tau_R \Leftrightarrow \tau_{R,\mathcal{C}}^* \geq 0$.

Finally, let us recall that, in the acoustic Riemann problem presented on Figure 2, $\rho_{L,\mathcal{A}}^* = \rho_L$ and $\rho_{R,\mathcal{A}}^* = \rho_R$. The intermediate densities are then already positive. No additional constraint on $a_{\mathcal{A}}$ needs to be provided in order to preserve the density positivity.

Appendix D

Relaxed Convective Subsystem

Once again, for the Riemann problem related to the convective relaxed subsystem $\mathcal{C}$, the specific internal energy reads:

$$\begin{aligned}
\varepsilon^*_{k,\mathcal{C}} &= e^*_{k,\mathcal{C}} - \frac{(u^*_{\mathcal{C}})^2}{2} \\
&= e_k - \frac{(u^*_{\mathcal{C}})^2}{2} + \mathscr{E}_0 \, \frac{(-1)^{i_k}}{a_{\mathcal{C}}} \, (\Pi^*_{\mathcal{C}} \, u^*_{\mathcal{C}} - \Pi_k \, u_k) \\
&= \varepsilon_k + \frac{u_k^2 - (u^*_{\mathcal{C}})^2}{2} + \mathscr{E}_0 \, \frac{(-1)^{i_k}}{a_{\mathcal{C}}} \, (\Pi^*_{\mathcal{C}} \, u^*_{\mathcal{C}} - \Pi_k \, u_k) \\
&= \varepsilon_k + \frac{u_k^2 + (u^*_{\mathcal{C}})^2}{2} + \mathscr{E}_0 \, \frac{(-1)^{i_k}}{a_{\mathcal{C}}} u^*_{\mathcal{C}} \left(\Pi^*_{\mathcal{C}} + \frac{(-1)^{i_k+1} \, a_{\mathcal{C}}}{\mathscr{E}_0} \, u^*_{\mathcal{C}} \right) - \mathscr{E}_0 \, \frac{(-1)^{i_k}}{a_{\mathcal{C}}} \, \Pi_k \, u_k
\end{aligned} \tag{100}$$

By combining, $u + (-1)^{i_k} \, \mathscr{E}_0 \, a_{\mathcal{C}} \, \tau$ and $\Pi + (a_{\mathcal{C}})^2 \, \tau$ which both are 1-Riemann invariants of subsystem $\mathcal{C}^\mu$, one can build a new one: $\Pi + \dfrac{(-1)^{i_k+1} \, a_{\mathcal{C}}}{\mathscr{E}_0} \, u$. Then, one can simplify the above expression of $\varepsilon^*_{k,\mathcal{C}}$, namely:

$$\begin{aligned}
\varepsilon^*_{k,\mathcal{C}} &= \varepsilon_k + \frac{u_k^2 + (u^*_C)^2}{2} + \mathscr{E}_0 \, \frac{(-1)^{i_k}}{a_{\mathcal{C}}} u^*_{\mathcal{C}} \left(\Pi_k + \frac{(-1)^{i_k+1} \, a_{\mathcal{C}}}{\mathscr{E}_0} \, u_k \right) - \mathscr{E}_0 \, \frac{(-1)^{i_k}}{a_{\mathcal{C}}} \, \Pi_k \, u_k \\
&= \varepsilon_k + \mathscr{E}_0 \, \frac{(-1)^{i_k}}{a_{\mathcal{C}}} \Pi_k \, (u^*_{\mathcal{C}} - u_k) + \frac{(u^*_{\mathcal{C}} - u_k)^2}{2}
\end{aligned} \tag{101}$$

Thus, a sufficient condition which would guarantee that $\forall k \in \{L, \, R\}\,, \; \varepsilon^*_{k,\mathcal{C}} \geq 0$ is:

$$\varepsilon_k + \mathscr{E}_0 \, \frac{(-1)^{i_k}}{a_{\mathcal{C}}} p_k \, (u^*_{\mathcal{C}} - u_k) \geq 0 \Leftrightarrow a^2_{\mathcal{C}} - \mathscr{E}_0 \, \rho^\varepsilon_k \frac{(u_R - u_L)}{2} \, a_{\mathcal{C}} + (-1)^{i_k+1} \mathscr{E}_0^2 \, \rho^\varepsilon_k \frac{(p_R - p_L)}{2} \geq 0 \tag{102}$$

with $\rho^\varepsilon_k = \dfrac{p_k}{\varepsilon_k}$, and considering that $p_k = \Pi_k$. Inequality (102) is very similar to the one obtained for the intermediate density positivity. The most demanding case is the one where $\forall k \in \{L, \, R\}\,, \; \Delta^\varepsilon_k \equiv \rho^\varepsilon_k \dfrac{(u_R - u_L)^2}{8} + (-1)^{i_k} \, (p_R - p_L) \geq 0$:

$$-\frac{\rho^\varepsilon_R \, (u_R - u_L)^2}{8} \leq p_R - p_L \leq \frac{\rho^\varepsilon_L \, (u_R - u_L)^2}{8} \tag{103}$$

Once again the highest roots related to the polynomial functions written in (102) are:

$$
\begin{aligned}
a^{\varepsilon}_{\mathcal{C},\,L} &\equiv \frac{\mathscr{E}_0}{2}\left(\frac{\rho^{\varepsilon}_L\,(u_R-u_L)}{2}+\sqrt{\frac{(\rho^{\varepsilon}_L)^2\,(u_R-u_L)^2}{4}-2\,\rho^{\varepsilon}_L\,(p_R-p_L)}\right)\\
a^{\varepsilon}_{\mathcal{C},\,R} &\equiv \frac{\mathscr{E}_0}{2}\left(\frac{\rho^{\varepsilon}_R\,(u_R-u_L)}{2}+\sqrt{\frac{(\rho^{\varepsilon}_R)^2\,(u_R-u_L)^2}{4}+2\,\rho^{\varepsilon}_R\,(p_R-p_L)}\right)
\end{aligned}
\tag{104}
$$

The sign of a^{ε}_L and a^{ε}_R is given by the following table:

	$u_R > u_L$	$u_R < u_L$
$p_R > p_L$	$a^{\varepsilon}_{\mathcal{C},\,L} > 0,\ a^{\varepsilon}_{\mathcal{C},\,R} > 0$	$a^{\varepsilon}_{\mathcal{C},\,L} < 0,\ a^{\varepsilon}_{\mathcal{C},\,R} > 0$
$p_R < p_L$	$a^{\varepsilon}_{\mathcal{C},\,L} > 0,\ a^{\varepsilon}_{\mathcal{C},\,R} > 0$	$a^{\varepsilon}_{\mathcal{C},\,L} > 0,\ a^{\varepsilon}_{\mathcal{C},\,R} < 0$

Table 6: Positivity Domain of $a^{\varepsilon}_{\mathcal{C},\,L}$ and $a^{\varepsilon}_{\mathcal{C},\,R}$

The non-dimensional version of these roots reads:

$$
\begin{aligned}
a^{\varepsilon}_{\mathcal{C},\,L} &\equiv \frac{\mathscr{E}_0}{2}\left(\frac{M\,\rho^{\varepsilon}_L\,(u_R-u_L)}{2}+\sqrt{\frac{M^2\,(\rho^{\varepsilon}_L)^2\,(u_R-u_L)^2}{4}-2\,\rho^{\varepsilon}_L\,(p_R-p_L)}\right)\\
a^{\varepsilon}_{\mathcal{C},\,R} &\equiv \frac{\mathscr{E}_0}{2}\left(\frac{M\,\rho^{\varepsilon}_R\,(u_R-u_L)}{2}+\sqrt{\frac{M^2\,(\rho^{\varepsilon}_R)^2\,(u_R-u_L)^2}{4}+2\,\rho^{\varepsilon}_R\,(p_R-p_L)}\right)
\end{aligned}
\tag{105}
$$

Then, unlike for the non-dimensional roots involved in the intermediate density positivity they are of order $O(\mathscr{E}_0)$. When either a^{ε}_L or a^{ε}_R are positive, they are injected in the subcaracteristic condition (37a).

Relaxed Acoustic Subsystem

The acoustic relaxed subsystem $\mathcal{A}^{\mu}$ also produces intermediate specific internal energies $\varepsilon^*_{k,\,\mathcal{A}} = e^*_{k,\,\mathcal{A}} - \dfrac{(u^*_{\mathcal{A}})^2}{2} = \varepsilon_k + \dfrac{(-1)^{i_k}}{a_{\mathcal{A}}}\Pi_k\ (u^*_{\mathcal{A}} - u_k) + \dfrac{(u^*_{\mathcal{A}} - u_k)^2}{2}$. The proof is similar to the one done for the convective relaxed subsystem. Sufficient conditions allowing to guarantee the intermediate specific energy positivity turns into the positivity of two polynomial functions of order two in $a_{\mathcal{A}}$. The most demanding case corresponds exactly to inequalities (103). Finally the roots above which the relaxation coefficient has to be are:

$$
a^{\varepsilon}_{\mathcal{A},\,L} \equiv \frac{a^{\varepsilon}_{\mathcal{C},\,L}}{\mathscr{E}_0};\ a^{\varepsilon}_{\mathcal{A},\,R} \equiv \frac{a^{\varepsilon}_{\mathcal{C},\,R}}{\mathscr{E}_0}.
\tag{106}
$$

Since for $k \in \{L,\,R\}$, $a^{\varepsilon}_{\mathcal{C},\,k} = O(\mathscr{E}_0)$, the non-dimensional expressions of $a^{\varepsilon}_{\mathcal{A},\,k}$ are of order one. One can notice that, in case of low-Mach flows, the constraint imposed by the relaxation convective subsystem on the specific internal energy positivity is negligible compared to the one of the relaxed acoustic subsystem. This is in agreement with the

formal non-dimensional asymptotic analysis made in **Subsection 3.2**: the convective subsystem converges formally toward a barotropic system where specific internal energy remains constant.

Appendix E

The below proof is only formal. It aims at exhibiting subcaracteristic conditions under which the relaxed subsystems contain diffusive operators. The latter would avoid instabilities which could prevent the convergence of the relaxation subsystems $\mathcal{C}^\mu$ and $\mathcal{A}^\mu$ towards $\mathcal{C}$ and $\mathcal{A}$.

Relaxed Convective Subsystem

Consider the relaxed convective subsystem $\mathcal{C}^\mu$:

$$\mathcal{C}^\mu : \begin{cases} \partial_t \rho + \partial_x (\rho u) = 0 \\ \partial_t \rho u + \partial_x (\rho u^2) + \partial_x \left(\mathscr{E}_0^2(t) \Pi \right) = 0 \\ \partial_t \rho e + \partial_x \left((\rho e + \mathscr{E}_0^2(t) \Pi) u \right) = 0 \\ \partial_t \Pi + u \partial_x \Pi + \dfrac{a_{\mathcal{C}}^2}{\rho} \partial_x u = \dfrac{1}{\mu} (p - \Pi) \end{cases} \tag{107}$$

Define $\mathbf{W} = [\rho, \rho u, \rho e, \rho \Pi]^T$ and $\mathbf{U} = [\rho, \rho u, \rho e]^T$. Assume that one can perform a Chapman-Enskog expansion on $\mathbf{U}$ and Π and write them in powers of μ, namely:

$$\begin{aligned} &\mathbf{U} = \mathbf{U}_0 + \mu \mathbf{U}_1 + O(\mu^2), \\ &\Pi = p(\mathbf{U}_0) + \mu \Pi_1 + O(\mu^2), \end{aligned} \tag{108}$$

with $\mathbf{U}_0$ and $p(\mathbf{U}_0)$ solutions of subsystem $\mathcal{C}$ and $\mathbf{U}_1$, Π_1 of order one. Making μ tend formally toward zero, the relaxed pressure equation becomes at order zero:

$$\partial_t p(\mathbf{U}_0) + u_0 \partial_x p(\mathbf{U}_0) + \frac{a_{\mathcal{C}}^2}{\rho_0} \partial_x u_0 = -\Pi_1 \Leftrightarrow \left(\frac{a_{\mathcal{C}}^2}{\rho_0} - \rho_0 c_{\mathcal{C}}(\mathbf{U}_0)^2 \right) \partial_x u_0 = -\Pi_1 \tag{109}$$

In order to make $\mathcal{C}^\mu$ converge towards $\mathcal{C}$, a basic step is to make sure that $\mathbf{U}_1$ remains of order one throughout time. Its evolution is influenced by non linear convective effects which mix order zero and order one terms as well as pressure effects related to $\mathscr{E}_0^2 \partial_x \Pi_1$ for the momentum equation and $\mathscr{E}_0^2 \partial_x (\Pi_1 u_0 + p_0 u_1)$ for the energy equation. Using equation (109), one can notice that:

$$-\mathscr{E}_0^2 \partial_x \Pi_1 = \mathscr{E}_0^2 \partial_x \left(\left(\frac{a_{\mathcal{C}}^2}{\rho_0} - \rho_0 c_{\mathcal{C}}(\mathbf{U}_0)^2 \right) \partial_x u_0 \right) \tag{110}$$

Thus, under the convective subcaracteristic condition $a_{\mathcal{C}} > \rho_0\, c_{\mathcal{C}}(\mathbf{U}_0)$, order zero terms results in a *diffusive* effect on the order one momentum equation. One can believe that this diffusion will be sufficient to prevent $\mathbf{U}_1$ from exploding when μ tends toward zero.

Relaxed Acoustic Subsystem

The same argumentation can be done on the relaxed acoustic subsystem $\mathcal{A}^{\mu}$. It gives the expected subcaracteristic condition (37b).

Appendix F

According to the truncation error analyses derived in **Section 5**, the scheme Sp-(M)-corr allows to reduce the spatial numerical diffusion in the convective as well as in the acoustic subsystem in the case of low-Mach number flows. On Figure 13 velocity profiles are plotted for different meshes. The diffusion reduction results in non-physical oscillations in the tail of the left rarefaction wave. However, the L^{∞} and the L^{1} norms of the induced error decay as the cells number increases. Hence, the scheme is stable and converges to the analytical solution.

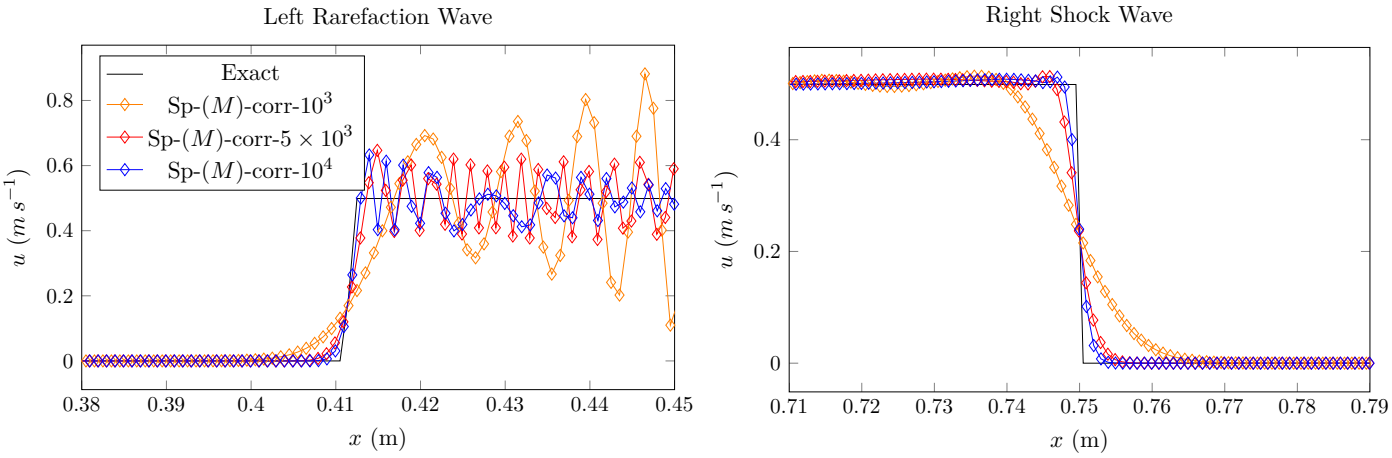

Figure 13: Velocity profile at $M = 4.2 \times 10^{-3}$, Sp-(M)-corr

Appendix G

Truncation Error of the Convective Subsystem

Let us consider the convective numerical flux located at face indexed by $i + 1/2$. For the sake of notations simplicity and in order to adopt an unstructured formalism, let us rewrite the index $i + 1/2$ as f for "face". Finally let us call L (respectively R) the index of the left (respectively the right) neighbor cell of the face f. Typically, in 1D $L = i$ and $R = i + 1$.

As mentioned in **Subsection 4.2.1** the relaxation scheme for the convective subsystem can be written:

$$\begin{aligned}\mathbf{H_c}_f^n = \mathbf{H_c}^n(\mathbf{U}_L,\,\mathbf{U}_R) = \frac{1}{2}\,\left(L(\mathbf{F}_{\mathcal{C}}^{\mu})\,(\mathbf{U}_L) + L(\mathbf{F}_{\mathcal{C}}^{\mu})\,(\mathbf{U}_R)\right) &- \frac{1}{2}\,|u_L - \mathscr{E}_0\,a_{\mathcal{C}}\,\tau_L|\,\left(\mathbf{U}_f^* - \mathbf{U}_L\right)\\ &- \frac{1}{2}\,|u_C^*|\,\left(\mathbf{U}_f^{**} - \mathbf{U}_f^*\right)\\ &- \frac{1}{2}\,|u_R + \mathscr{E}_0\,a_{\mathcal{C}}\,\tau_R|\,\left(\mathbf{U}_R - \mathbf{U}_f^{**}\right)\\ L(\mathbf{F}_{\mathcal{C}}^{\mu})\,(\mathbf{U}) = \left[\rho\,u,\,\rho\,u^2 + \mathscr{E}_0^2\,p,\,(\rho\,e + \mathscr{E}_0^2\,p)\,u\right]^T &\end{aligned} \tag{111}$$

Using the classical rescaling presented on **Section 3** the non-dimensional version of this numerical flux writes:

$$\begin{aligned}\mathbf{H_c}_f^n = \mathbf{H}^n(\mathbf{U}_L,\,\mathbf{U}_R) = \frac{1}{2}\,\left(L(\mathbf{F}_{\mathcal{C}}^{\mu})\,(\mathbf{U}_L) + L(\mathbf{F}_{\mathcal{C}}^{\mu})\,(\mathbf{U}_R)\right) &- \frac{1}{2}\left|u_L - \frac{\mathscr{E}_0}{M}\,a_{\mathcal{C}}\,\tau_L\right|\,\left(\mathbf{U}_f^* - \mathbf{U}_L\right)\\ &- \frac{1}{2}\,|u_C^*|\,\left(\mathbf{U}_f^{**} - \mathbf{U}_f^*\right)\\ &- \frac{1}{2}\left|u_R + \frac{\mathscr{E}_0}{M}\,a_{\mathcal{C}}\,\tau_R\right|\,\left(\mathbf{U}_R - \mathbf{U}_f^{**}\right)\\ L(\mathbf{F}_{\mathcal{C}}^{\mu})\,(\mathbf{U}) = \left[\rho\,u,\,\rho\,u^2 + (\mathscr{E}_0/M)^2\,p,\,(\rho\,e + \mathscr{E}_0^2\,p)\,u\right]^T,\;\rho\,e = \rho\,\varepsilon + \frac{M^2}{2}\,\rho\,u^2 &\end{aligned} \tag{112}$$

For the sake of notations, let us rewrite $\mathbf{U}_f^*$ as $\mathbf{U}_L^*$ and $\mathbf{U}_f^{**}$ as $\mathbf{U}_R^*$. The non-dimensional intermediate states $\mathbf{U}_k^*,\;k \in \{L,\,R\}$ can be expressed as:

$$\mathbf{U}_k^* = \begin{bmatrix}\rho_{k,\mathcal{C}}^*\\ \rho_{k,\mathcal{C}}^*\,u_C^*\\ \rho_{k,\mathcal{C}}^*\,e_{k,\mathcal{C}}^*\end{bmatrix} \tag{113}$$

with:

$$\begin{cases} u_C^* = \dfrac{u_R + u_L}{2} - \dfrac{\mathscr{E}_0}{M}\dfrac{(p_R - p_L)}{2\,a_{\mathcal{C}}}\\ p^* = \dfrac{p_R + p_L}{2} - \dfrac{M}{\mathscr{E}_0}\dfrac{a_{\mathcal{C}}\;(u_R - u_L)}{2}\\ \rho_{k,\mathcal{C}}^* = 1/\tau_k^*,\;\tau_k^* = \tau_k + \dfrac{M}{\mathscr{E}_0}\dfrac{(-1)^{i_k+1}}{a_{\mathcal{C}}}\,(u_C^* - u_k)\\ e_{k,\mathcal{C}}^* = e_k + \mathscr{E}_0\,M\,\dfrac{(-1)^{i_k}}{a_{\mathcal{C}}}\,(p^*\,u_C^* - p_k\,u_k)\\ a_{\mathcal{C}} = K \cdot max\left(\rho_L\,c_{\mathcal{C}}(\rho_L,\,p_L),\,\rho_R\,c_{\mathcal{C}}(\rho_R,\,p_R)\right),\;K > 1\\ k \in \{L,\,R\},\;i_L \equiv 1,\;i_R \equiv 2 \end{cases} \tag{114}$$

Let us define x_f, x_L and x_R the positions of the face, left cell and right cell barycenters. In 1D: $x_L = x_i$, $x_R = x_{i+1}$ and $x_f = x_L + \Delta x/2 = x_R - \Delta x/2$. At a given time t, for a smooth function $\phi(.,t)$ let us write ϕ_f for $\phi(x_f,\, t)$ and ϕ_L for $\phi(x_L,\, t)$. Particularly, we will consider $x \to a(x,t)$ a smooth function such that $a_{\mathcal{C}}(x_{i+1/2}, t^n) = (a_{\mathcal{C}})^n_{i+1/2}$.

Let us consider a non-dimensional smooth state $(x,t) \to \mathbf{U}(x,t)$ verifying:

$$\frac{\mathbf{U}(x_i,\, t^n + \Delta t) - \mathbf{U}(x_i,\, t^n)}{\Delta t} + \frac{\mathbf{H_c}\left(\mathbf{U}(x_i,\, t^n),\, \mathbf{U}(x_{i+1},\, t^n)\right) - \mathbf{H_c}\left(\mathbf{U}(x_{i-1},\, t^n),\, \mathbf{U}(x_i,\, t^n)\right)}{\Delta x} = 0 \tag{115}$$

One wonders which partial differential equation does such a smooth solution verify?

It can be first noticed that $\dfrac{\mathbf{U}(x_i,\, t^n + \Delta t) - \mathbf{U}(x_i,\, t^n)}{\Delta t}$ is consistent with $\partial_t\, \mathbf{U}_i + \underline{O}\,(\Delta t)$.

Let us now focus on ${\mathbf{H_c}}^n(\mathbf{U}_L,\, \mathbf{U}_R)$: first, $\forall k \in \{L,\, R\}$:

$$\mathbf{U}^*_k - \mathbf{U}_k = \begin{bmatrix} \rho^*_{k,\mathcal{C}} - \rho_k \\ (\rho^*_{k,\mathcal{C}} - \rho_k)\, u^*_C + \rho_k\, (u^*_C - u_k) \\ (\rho^*_{k,\mathcal{C}} - \rho_k)\, e^*_{k,\mathcal{C}} + \rho_k\, (e^*_{k,\mathcal{C}} - e_k) \end{bmatrix} \tag{116}$$

Furthermore, performing a Taylor expansion around x_f, and setting $i_L = 1$, $i_R = 2$, one obtains:

$$\begin{cases} \rho^*_{k,\mathcal{C}} - \rho_k = \left[-\dfrac{\rho_f^2}{a_f} \left(\dfrac{M}{\mathscr{E}_0}\right) \partial_x\, u_{|f} + (-1)^{i_k+1} \left(\dfrac{\rho_f}{a_f}\right)^2 \partial_x\, p_{|f} \right] \dfrac{\Delta x}{2} + O\left((1 + \dfrac{M}{\mathscr{E}_0}) \Delta x^2 \right) \\ u^*_C - u_k = \left[(-1)^{i_k+1} \partial_x\, u_{|f} - \left(\dfrac{\mathscr{E}_0}{M}\right) \dfrac{1}{a_f} \partial_x\, p_{|f} \right] \dfrac{\Delta x}{2} + O\left((1 + \dfrac{\mathscr{E}_0}{M}) \Delta x^2 \right) \\ e^*_{k,\mathcal{C}} - e_k = M\, \mathscr{E}_0 \left[-\dfrac{1}{a_f} \partial_x\, p\, u_{|f} + (-1)^{i_k+1} \left(\left(\dfrac{\mathscr{E}_0}{M}\right) \dfrac{p_f}{a_f^2} \partial_x\, p_{|f} + \left(\dfrac{M}{\mathscr{E}_0}\right) u_f \partial_x\, u_{|f} \right) \right] \dfrac{\Delta x}{2} \\ \qquad\qquad + O\left(M\, \mathscr{E}_0 (1 + \dfrac{\mathscr{E}_0}{M} + \dfrac{M}{\mathscr{E}_0}) \Delta x^2 \right) \\ \qquad u^*_C = u_f - \left(\dfrac{\mathscr{E}_0}{M}\right) \dfrac{1}{a_f} \partial_x\, p_{|f} \dfrac{\Delta x}{2} + O\left((1 + \dfrac{\mathscr{E}_0}{M}) \Delta x^2 \right) \\ \qquad e^*_{k,\mathcal{C}} = e_f + (-1)^{i_k} \partial_x\, e_{|f} \dfrac{\Delta x}{2} + e^*_{k,\mathcal{C}} - e_k \end{cases} \tag{117}$$

Then:

$$\mathbf{U}_k^* - \mathbf{U}_k = \frac{\Delta x}{2}\begin{bmatrix} -\frac{\rho_f^2}{a_f}\left(\frac{M}{\mathscr{E}_0}\right)\partial_x u_{|f} + (-1)^{i_k+1}\left(\frac{\rho_f}{a_f}\right)^2 \partial_x p_{|f} \\ \rho_f\left((-1)^{i_k+1} - \frac{\rho_f u_f}{a_f}\frac{M}{\mathscr{E}_0}\right)\partial_x u_{|f} + \frac{\rho_f}{a_f}\left((-1)^{i_k+1}\frac{\rho_f uf}{a_f} - \frac{\mathscr{E}_0}{M}\right)\partial_x p_{|f} \\ \rho_f e_f\left(\left(\frac{\rho_f}{a_f}\frac{M}{\mathscr{E}_0} + (-1)^{i_k+1}\frac{u_f}{e_f}\mathscr{E}_0\frac{M}{\mathscr{E}_0}\right)\partial_x u_{|f} + (-1)^{i_k+1}\left(\frac{\rho_f}{a_f^2} + \mathscr{E}_0\frac{\mathscr{E}_0}{M}\frac{p_f}{a_f^2 e_f}\right)\partial_x p_{|f}\right) \\ +\mathscr{E}_0\frac{\mathscr{E}_0}{M}\frac{p_f}{a_f^2 e_f}\partial_x p\, u_{|f} \end{bmatrix} + \underline{O}\left((1 + \frac{\mathscr{E}_0}{M} + \frac{M}{\mathscr{E}_0})\Delta x^2\right) \tag{118}$$

One can finally observe that, for the terms in order one in space, the Mach number is always compensated with the weighting parameter $\mathscr{E}_0$. Thus $\forall k \in \{L,\, R\}$:

$$\mathbf{U}_k^* - \mathbf{U}_k = \underline{O}\left((1 + \frac{\mathscr{E}_0}{M} + \frac{M}{\mathscr{E}_0})\Delta x\right)_f \tag{119}$$

Similarly:

$$\begin{aligned} \mathbf{U}_R^* - \mathbf{U}_L^* &= (\mathbf{U}_R^* - \mathbf{U}_R) + (\mathbf{U}_R - \mathbf{U}_L) + (\mathbf{U}_L - \mathbf{U}_L^*) \\ &= \underline{O}\left((1 + \frac{\mathscr{E}_0}{M} + \frac{M}{\mathscr{E}_0})\Delta x\right)_f \end{aligned} \tag{120}$$

Furthermore, one can easily see that $\forall k \in \{L,\, R\}$:

$$\begin{aligned} \left|u_k + (-1)^{i_k}\frac{\mathscr{E}_0}{M}a_{\mathcal{C}}\,\tau_k\right| &= \left|u_f + (-1)^{i_k}\frac{\mathscr{E}_0}{M}a_f\,\tau_f\right| + O\left((1 + \frac{\mathscr{E}_0}{M})\Delta x\right) \\ |u_C^*| &= |u_f| + O\left((1 + \frac{\mathscr{E}_0}{M})\Delta x\right) \end{aligned} \tag{121}$$

Thus, at a given face f we have:

$$\mathbf{H_c}_f^n = \mathbf{H_c}^n(\mathbf{U}_L,\, \mathbf{U}_R) = \frac{1}{2}\left(L(\mathbf{F}_{\mathcal{C}}^{\mu})\,(\mathbf{U}_L) + L(\mathbf{F}_{\mathcal{C}}^{\mu})\,(\mathbf{U}_R)\right) + \underline{O}\left((1 + \frac{\mathscr{E}_0}{M} + \frac{M}{\mathscr{E}_0})\Delta x\right)_f \tag{122}$$

Besides, $\frac{1}{2}\left(L(\mathbf{F}_{\mathcal{C}}^{\mu})\,(\mathbf{U}_L) + L(\mathbf{F}_{\mathcal{C}}^{\mu})\,(\mathbf{U}_R)\right)$ is consistent with $L(\mathbf{F}_{\mathcal{C}}^{\mu})\,(\mathbf{U}_f) + \underline{O}\left(\Delta x^2\right)$.
Finally $\frac{\mathbf{H}_{i+1/2}^n - \mathbf{H}_{i-1/2}^n}{\Delta x}$ is consistent with $\partial_x\ L(\mathbf{F}_{\mathcal{C}}^{\mu})\,(\mathbf{U}_i) + \underline{O}\left((1 + \frac{\mathscr{E}_0}{M} + \frac{M}{\mathscr{E}_0})\Delta x\right)$. Thus we have found that the smooth solution $\mathbf{U}(x,\, t)$ verified the PDE $\forall x_i,\, t^n$:

$$\partial_t\ \mathbf{U}_i^n + \partial_x\ L(\mathbf{F}_{\mathcal{C}}^{\mu})\,(\mathbf{U}_i^n) = \underline{O}\,(\Delta t) + \underline{O}\left((1 + \frac{\mathscr{E}_0}{M} + \frac{M}{\mathscr{E}_0})\Delta x\right) \tag{123}$$

Truncation Error of the Acoustic Subsystem

Keeping the same notations than previously, the non-dimensional relaxation flux for the acoustic subsystem writes:

$$\mathbf{H_{ac}}_f^n = \left(1-\mathscr{E}_0^2\right)\begin{bmatrix}0\\ \Pi_{\mathcal{A}}^*\\ \Pi_{\mathcal{A}}^*\,u_{\mathcal{A}}^*\end{bmatrix} = \left(1-\mathscr{E}_0^2\right)\left(\begin{bmatrix}0\\ \frac{1}{M^2}\frac{p_R+p_L}{2}\\ \frac{p_R\,u_R+p_L\,u_L}{2}\end{bmatrix} - \begin{bmatrix}0\\ \frac{1}{M}\frac{a_{\mathcal{A}}}{2}\,(u_R-u_L)\\ \frac{M\,a_{\mathcal{A}}}{4}\left(u_R^2-u_L^2\right)+\frac{1}{4}\frac{1}{M\,a_{\mathcal{A}}}\left(p_R^2-p_L^2\right)\end{bmatrix}\right)$$
$$\text{with: } a_{\mathcal{A}} = K\cdot max\left(\rho_L\,c_{\mathcal{A}}(\rho_L,\,p_L),\,\rho_R\,c_{\mathcal{A}}(\rho_R,\,p_R)\right),\ K>1 \tag{124}$$

It is easy to check that $\left(1-\mathscr{E}_0^2\right)\begin{bmatrix}0\\ \frac{1}{M^2}\frac{p_R+p_L}{2}\\ \frac{p_R\,u_R+p_L\,u_L}{2}\end{bmatrix}$ is consistent with $\left(1-\mathscr{E}_0^2\right)\begin{bmatrix}0\\ \frac{p_f}{M^2}\\ p_f\,u_f\end{bmatrix}+\begin{bmatrix}0\\ O\left((1-\mathscr{E}_0^2)(\Delta x/M)^2\right)\\ O\left((1-\mathscr{E}_0^2)\Delta x^2\right)\end{bmatrix}$. Besides, $-(1-\mathscr{E}_0^2)\begin{bmatrix}0\\ \frac{1}{M}\frac{a_{\mathcal{A}}}{2}\,(u_R-u_L)\\ \frac{M\,a_{\mathcal{A}}}{4}\left(u_R^2-u_L^2\right)+\frac{1}{4}\frac{1}{M\,a_{\mathcal{A}}}\left(p_R^2-p_L^2\right)\end{bmatrix}$ is consistent with $-(1-\mathscr{E}_0^2)\frac{\Delta x}{2}\begin{bmatrix}0\\ \frac{1}{M}a_f\partial_x\,u_{|f}\\ M\,a_f\,u_f\partial_x\,u_{|_f}+\frac{1}{M\,a_f}\,p_f\partial_x\,p_{|f}\end{bmatrix}+\begin{bmatrix}0\\ O\left(\frac{(1-\mathscr{E}_0^2)}{M}\Delta x^2\right)\\ O\left((1-\mathscr{E}_0^2)(M+\frac{1}{M})\Delta x^2\right)\end{bmatrix}_f$.

Finally, one obtains at order one in space:

$$\mathbf{H_{ac}}_f^n = \left(1-\mathscr{E}_0^2\right)\begin{bmatrix}0\\ \frac{p_f}{M^2}\\ p_f\,u_f\end{bmatrix}+\begin{bmatrix}0\\ O\left(\frac{(1-\mathscr{E}_0^2)}{M}\Delta x\right)\\ O\left((1-\mathscr{E}_0^2)(M+\frac{1}{M})\Delta x\right)\end{bmatrix}_f \tag{125}$$

Thus we have found that the smooth solution $\underline{U}(x,\,t)$ verified the PDE $\forall x_i,\,t^n$:

$$\begin{aligned}
&\partial_t\,\rho = O(\Delta t)\\
&\partial_t\,(\rho\,u)+\partial_x\,\left((1-\mathscr{E}_0^2(t))\,p\right) = O(\Delta t)+O\left(\frac{(1-\mathscr{E}_0^2)}{M})\Delta x\right)\\
&\partial_t\,(\rho\,e)+\partial_x\,\left((1-\mathscr{E}_0^2(t))\,p\,u\right) = O(\Delta t)+O\left((1-\mathscr{E}_0^2)(M+\frac{1}{M})\Delta x\right)
\end{aligned} \tag{126}$$

The non-dimensional version of the CFL condition (58) reads:

$\Delta t^n < \dfrac{M\,\Delta x}{\underset{i+1/2}{max}\left(|u_i^n| + c_i^n,\, \left|u_{i+1}^n\right| + c_{i+1}^n\right)}$. Thus $O(\Delta t)$ is actually a $O(M\Delta x)$. Injected in equations (123) and (126), we obtain the results of proposition 2 and proposition 3.

Truncation Error of the Acoustic Subsystem with low-Mach Correction

Endowed with the low-Mach correction described in equation (74), the acoustic flux at face x_f reads:

$$\mathbf{H_{ac}}_f^n = \left(1-\mathscr{E}_0^2\right)\begin{bmatrix}0\\ \Pi^*\\ \Pi^*\,u^*\end{bmatrix} = \left(1-\mathscr{E}_0^2\right)\left(\begin{bmatrix}0\\ \dfrac{1}{M^2}\dfrac{\Pi_R+\Pi_L}{2}\\ \dfrac{\Pi_R\,u_R+\Pi_L\,u_L}{2}\end{bmatrix} - \begin{bmatrix}0\\ \dfrac{\theta}{M}\dfrac{a_{\mathcal{A}}}{2}\left(u_R-u_L\right)\\ \dfrac{M\theta\,a_{\mathcal{A}}}{4}\left(u_R^2-u_L^2\right)+\dfrac{1}{4}\dfrac{1}{M\,a_{\mathcal{A}}}\left(\Pi_R^2-\Pi_L^2\right)\end{bmatrix}\right) \tag{127}$$

The correction part is now consistent with:

$$-(1-\mathscr{E}_0^2)\frac{\Delta x}{2}\begin{bmatrix}0\\ \dfrac{\theta_f}{M}a_f\partial_x\,u_{|f}\\ M\theta_f\,a_f\,u_f\partial_x\,u_{|_f}+\dfrac{1}{M\,a_f}\,p_f\partial_x\,p_{|f}\end{bmatrix} + \begin{bmatrix}0\\ O\left(\dfrac{(1-\mathscr{E}_0^2)\,\theta}{M}\Delta x^2\right)\\ O\left((1-\mathscr{E}_0^2)(M\,\theta+\dfrac{1}{M})\Delta x^2\right)\end{bmatrix}_f.$$

At order one in space:

$$\mathbf{H_{ac}}_f^n = \left(1-\mathscr{E}_0^2\right)\begin{bmatrix}0\\ \dfrac{p_f}{M^2}\\ p_f\,u_f\end{bmatrix} + \begin{bmatrix}0\\ O\left(\dfrac{(1-\mathscr{E}_0^2)\theta}{M}\Delta x\right)\\ O\left((1-\mathscr{E}_0^2)(M\theta+\dfrac{1}{M})\Delta x\right)\end{bmatrix}_f \tag{128}$$

For a smooth solution $\underline{U}(x,\,t)$, the truncation error analysis made on the acoustic scheme with low-Mach correction gives $\forall x_i,\, t^n$:

$$\begin{aligned}
&\partial_t\,\rho = O(\Delta t)\\
&\partial_t\,(\rho\,u) + \partial_x\,\left((1-\mathscr{E}_0^2(t))\,p\right) = O(\Delta t) + O\left(\frac{(1-\mathscr{E}_0^2)\theta}{M})\Delta x\right)\\
&\partial_t\,(\rho\,e) + \partial_x\,\left((1-\mathscr{E}_0^2(t))\,p\,u\right) = O(\Delta t) + O\left((1-\mathscr{E}_0^2)(M\theta+\frac{1}{M})\Delta x\right)
\end{aligned} \tag{129}$$

Truncation Error of the Global Relaxation Scheme

Consider the overall relaxation scheme described in equation (56). Thanks to the truncation error analysis of the convective subsystem one can notice that:

$$
\begin{aligned}
\mathbf{U}_i^{n+} &= \mathbf{U}_i^n - \partial_x \, \mathbf{F}_{\mathcal{C}}^{\mu}\left(\mathbf{U}_i^n\right) \, \Delta t + \underline{O}\left((1 + \frac{\mathscr{E}_0}{M} + \frac{M}{\mathscr{E}_0})\Delta x \, \Delta t\right) \\
&= \mathbf{U}_i^n - \partial_x \, \mathbf{F}_{\mathcal{C}}^{\mu}\left(\mathbf{U}_i^n\right) \, A^n M \Delta x + \underline{O}\left(M(1 + \frac{\mathscr{E}_0}{M} + \frac{M}{\mathscr{E}_0})\Delta x^2\right) \\
\text{with: } A^n &= \frac{\sigma}{\underset{i+1/2}{max}\left(|u_i^n| + c_i^n, \left|u_{i+1}^n\right| + c_{i+1}^n\right)}, \, \sigma < 1
\end{aligned}
\tag{130}
$$

Then, for order one in space, $\forall k \in \{L, \, R\}$: $\mathbf{U}_k^{n+} = \mathbf{U}_k^n + \underline{B}_k^n M \Delta x$, with $\underline{B}$ a continuous function of order one. Injecting $\mathbf{U}_k^{n+}$ into the non-dimensional acoustic flux detailed in equation (124), one can notice that the only contribution of order $(1 - \mathscr{E}_0^2)\frac{\Delta x}{M}$ brought by the fluctuation $\underline{B}_k^n M \Delta x$ is created by the centered pressure terms since:

$$
\begin{aligned}
\frac{1}{M^2}\frac{p^{EOS}\left(\mathbf{U}_R^{n+}\right) + p^{EOS}\left(\mathbf{U}_L^{n+}\right)}{2} &= \frac{1}{M^2}\left(p^{EOS}\left(\mathbf{U}_f^n\right) + \underline{\nabla}_U \, p^{EOS}\left(\mathbf{U}_f^n\right) \cdot \underline{B}_f^n M \Delta x + O(\Delta x^2)\right) \\
&= \frac{p_f^n}{M^2} + O\left(\frac{\Delta x}{M}\right) + O\left((\frac{\Delta x}{M})^2\right)
\end{aligned}
\tag{131}
$$

Thus, $\mathbf{H_{ac}}_{i+1/2}^n\left(\mathbf{U}_L^{n+}, \, \mathbf{U}_R^{n+}\right)$ is consistent with: $\left(1 - \mathscr{E}_0^2\right)\begin{bmatrix} 0 \\ \frac{p_f^n}{M^2} \\ p_f^n \, u_f^n \end{bmatrix} + \underline{O}\left((1 - \mathscr{E}_0^2)(1 + M + \frac{1}{M})\Delta x\right)_f$.

The end of the proof falls naturally.

References

[1] R. Baraille, G. Bourdin, F. Dubois, and A. Y. Le Roux. Une version à pas fractionnaires du schéma de Godunov pour l'hydrodynamique. *Compte Rendu de l'Académie des Sciences*, 314:147–152, 1992.

[2] M. Baudin, C. Berthon, F. Coquel, R. Masson, and Q. H. Tran. A Relaxation Method for Two-phase Flow Models with Hydrodynamic Closure Laws. *Numerische Mathematik*, 99:411–440, 2005.

[3] M. Baudin, F. Coquel, and Q. H. Tran. A Semi-Implicit Relaxation Scheme for Modelling Two-phase Flow in a Pipeline. *SIAM Journal of Scientific Computing*, 27:914–936, 2005.

[4] F. Bouchut. Entropy Satisfying Flux Vector Splittings and Kinetic BGK Models. *Numerische Mathematik*, 94:623–672, 2003.

[5] F. Bouchut. *Nonlinear Stability of Finite Volume Methods for Hyperbolic Conservation Laws*. Birkäser, 2004.

[6] T. Buffard and J-M. Hérard. A conservative fractional step method to solve non-isentropic Euler equations. *Computer Methods in Applied Mechanics and Engineering*, 144:199–225, 1996.

[7] C. Chalons and J.F. Coulombel. Relaxations approximation of the Euler equations. *Journal of Mathematical Analysis and Applications*, 348:872–893, 2008.

[8] C. Chalons, M. Girardin, and S. Kokh. An All-Regime Lagrange-Projection Like Scheme for the Gas Dynamics Equations on Unstructured Meshes. *Communications in Computational Physics*, 20:188–233, 2016.

[9] G. Q. Chen, C. D. Levermore, and T.-P. Liu. Hyperbolic Conservation Laws with Stiff Relaxation Terms and Entropy. *Communications on Pure and Applied Mathematics*, 47:787–830, 1994.

[10] S. Clerc. Numerical simulation of the homogeneous equilibrium model for two-phase flows. *Journal of Computational Physics*, 161:354–375, 1999.

[11] F. Coquel, E. Godlewski, B. Perthame, A. In, and P. Rascle. Some New Godunov and Relaxation Methods for Two-Phase Flow Problems. *Kluwer Academic/Plenum Publishers (New York)*, pages 179–188, 2001.

[12] F. Coquel, E. Godlewski, and N. Seguin. Relaxation of Fluid Systems. *Mathematical Models and Methods in Applied Science*, 22:43–95, 2012.

[13] F. Coquel, Q. L. Nguyen, M. Postel, and Q. H. Tran. Entropy-Satisfying Relaxation Method with Large Time-Steps for Euler IBVPS. *Mathematics of Computation*, 79:1493–1533, 2010.

[14] S. Dallet. . PhD thesis, Aix-Marseille Université, In preparation, 2017.

[15] F. Daude, F. Mary, and P. Comte. Self-adaptative Newton-based Iteration Strategy for the LES of Turbulent Multi-scale Flows. *Computers and Fluids*, 100:278–290, 2014.

[16] P. Degond and M. Tang. All Speed Scheme for the Low Mach Number Limit of the Isentropic Euler Equation. *Communications in Computational Physics*, 10:1–31, 2011.

[17] S. Dellacherie. Analysis of Godunov type schemes applied to the compressible Euler system at low Mach number. *Journal of Computational Physics*, 229:978–1016, 2009.

[18] S. Dellacherie, P. Omnes, J. Jung, and P.A. Raviart. Construction of modified Godunov type schemes accurate at any Mach number for the compressible Euler system. *Mathematical Models and Methods in Applied Science*, 26:2525–2615, 2016.

[19] G. Dimarco, R. Loubère, and M-H. Vignal. Study of a New Asymptotic Preserving Scheme for the Euler System in the Low Mach Number Limit. *Preprint*, https://hal.archives-ouvertes.fr/hal-01297238, 2016.

[20] T. Gallouët, J-M Hérard, and N. Seguin. Some Recent Finite Volume Schemes to Compute Euler Equations Using Real Gas EOS. *International Journal for Numerical Methods in Fluids*, 39:1073–1138, 2002.

[21] T. Gallouët, J-M Hérard, and N. Seguin. Numerical modeling of two-phase flows using the two-fluid two-pressure approach. *Mathematical Models and Methods in Applied Sciences*, 14:663–700, 2004.

[22] M. Girardin. *Asymptotic preserving and all-regime Lagrange-Projection like numerical schemes: application to two-phase flows in low Mach regime.* PhD thesis, Université Pierre et Marie Curie, https://tel.archives-ouvertes.fr/tel-01127428, 2015.

[23] E. Godlewski and P.A. Raviart. *Numerical Approximation of Hyperbolic Systems of Conservation Laws.* Springer, 1996.

[24] H. Guillard and A. Murrone. On the Behavior of Upwind Schemes in the Low Mach Number Limit: II Godunov type schemes. *Computers and Fluids*, 33:655–675, 2004.

[25] H. Guillard and C. Viozat. On the Behavior of Upwind Schemes in the Low Mach Number Limit. *Computers and Fluids*, 28:63–86, 1999.

[26] J. Haack, S. Jin, and J. G. Liu. An All-speed Asymptotic-preserving Method for the Isentropic Euler and Navier-Stokes Equations. *Communications in Computational Physics*, 12:955–980, 2012.

[27] A. Harten, P. D. Lax, and B. Van Leer. On upstream differencing and Godunov-type schemes for hyperbolic conservation laws. *SIAM Review*, 25:35–61, 1983.

[28] D. Iampietro, F. Daude, P. Galon, and J. M. Hérard. A Weighted Splitting Approach For Low-Mach Number Flows. *Submitted to FVCA 8 proceedings*, 2017.

[29] D. Iampietro, F. Daude, P. Galon, and J. M. Hérard. An Implicit-Explicit Fractional Step Approach Adapted to Weakly Compressible Fluid Flows. *To be submitted*, 2017.

[30] S. Jin and Z.-P. Xin. The Relaxation Schemes for Systems of Conservation Laws in Arbitrary Dimensions. *Communications on Pure and Applied Mathematics*, 48:235–276, 1995.

[31] M. S. Liou and C. J. Steffen. A New Flux Splitting Scheme. *Journal of Computational Physics*, 107:23–39, 1993.

[32] M. P. Martín and G. V. Candler. A Parallel Implicit Method for the Direct Numerical Simulation of Wall-bounded Compressible Turbulence. *Journal of Computational Physics*, 215:153–171, 2006.

[33] S. Schochet and G. Metivier. Fast Singular Limits of Hyperbolic PDEs. *Journal of Differential Equations*, 114:476–512, 1994.

[34] S. Schochet and G. Metivier. Limite incompressible des équations d' Euler non-isentropiques. *Preprint, https://www.math.u-bordeaux.fr/ gmetivie/Preprints.html*, 2000.

[35] S. Schochet and G. Metivier. The Incompressible Limit of Euler Non-isentropic Equations. *Archive for Rational Mechanics and Analysis*, 158:61–90, 2001.

[36] A. R. Simpson and E. B. Wylie. Large Water-hammer Pressures for Column Separation in Pipelines. *Journal of Hydraulic Engineering*, 117:1310–1316, 1991.

[37] J. Smoller. *Shock Waves and Reaction-Diffusion Equations*. Springer-Verlag, 1994.

[38] G. A. Sod. *Numerical methods in fluid dynamics, Initial and initial-boundary value problems*. Cambridge University Press, 1985.

[39] I. Suliciu. On the thermodynamics of fluids with relaxation and phase transitions. *International Journal of Engineering Science*, 36:921–947, 1998.

[40] S. Tan and Q. Li. Time-Implicit Gas-Kinetic Scheme. *Computers and Fluids*, 144:44–59, 2017.

[41] E. F. Toro and M. E. Vazquez-Cendon. Flux Splitting Schemes for the Euler Equations. *Computers and Fluids*, 70:1–12, 2012.

[42] E.F. Toro. *Riemann Solvers and Numerical Methods for Fluid Dynamics*. Springer, 1999.

[43] E. Turkel. Preconditioned methods for solving the incompressible and low speed compressible equations. *Journal of Computational Physics*, 72:277–298, 1987.

[44] J. B. Whitham. *Linear and Non Linear Waves*. John Wiley & Sons Inc, 1974.

[45] G-C. Zha and E. Bilgen. Numerical Solution of Euler Equations by a New Flux Vector Splitting Scheme. *International Journal of Numerical Methods in Fluids*, 17:115–44, 1993.